2007

The Marine Stratus/Stratocumulus Experiment (MASE): Aerosol-cloud relationships in marine stratocumulus

Lu, Miao-Lu

The Marine Stratus/Stratocumulus Experiment (MASE): Aerosol-cloud relationships in marine stratocumulus

Miao-Ling Lu,[1] William C. Conant,[2] Haflidi H. Jonsson,[3] Varuntida Varutbangkul,[4] Richard C. Flagan,[5] and John H. Seinfeld[5]

Received 29 August 2006; revised 1 December 2006; accepted 26 January 2007; published 22 May 2007.

[1] The Marine Stratus/Stratocumulus Experiment (MASE) field campaign was undertaken in July 2005 off the coast of Monterey, California to evaluate aerosol-cloud relationships in the climatically important regime of eastern Pacific marine stratocumulus. Aerosol and cloud properties were measured onboard the Center for Interdisciplinary Remotely-Piloted Aircraft Studies (CIRPAS) Twin Otter aircraft. One cloud that was clearly impacted by ship emissions as well as the ensemble of clouds observed over the entire mission are analyzed in detail. Results at both the individual and ensemble scales clearly confirm the Twomey effect (first indirect effect of aerosols) and demonstrate drizzle suppression at elevated aerosol number concentration. For the ship track impacted cloud, suppressed drizzle in the track led to a larger cloud liquid water path (LWP) at the same cloud thickness, in accord with the so-called second indirect effect. Ensemble averages over all clouds sampled over the entire 13-flight mission show the opposite effect of aerosol number concentration on LWP, presumably the result of other dynamic influences (e.g., updraft velocity and ambient sounding profile). Individual polluted clouds were found to exhibit a narrower cloud drop spectral width in accord with theoretical prediction (M.-L. Lu and J. H. Seinfeld, Effect of aerosol number concentration on cloud droplet dispersion: A large-eddy simulation study and implications for aerosol indirect forcing, *Journal of Geophysical Research*, 2006). This field experiment demonstrates both the indirect aerosol effect on ship track perturbed clouds, as well as the subtleties involved in extracting these effects over an ensemble of clouds sampled over a 1-month period.

Citation: Lu, M.-L., W. C. Conant, H. H. Jonsson, V. Varutbangkul, R. C. Flagan, and J. H. Seinfeld (2007), The Marine Stratus/Stratocumulus Experiment (MASE): Aerosol-cloud relationships in marine stratocumulus, *J. Geophys. Res.*, *112*, D10209, doi:10.1029/2006JD007985.

1. Introduction

[2] One of the largest uncertainties in quantitative estimates of radiative forcing of the climate system is the interaction between aerosols and clouds, the so-called aerosol indirect effect [Intergovernmental Panel on Climate Change (IPCC), 2001; *Lohmann and Feichter*, 2005]. Aerosol indirect forcing of liquid (warm) clouds has generally been divided into two types. The first type, also referred to as the Twomey effect [*Twomey*, 1977], is that in which an increase in the number of subcloud aerosols at constant liquid water content leads to more numerous, smaller cloud droplets and a more reflective cloud. This effect, referred to as the first indirect effect, has strong observational support from in situ measurements [*Warner and Twomey*, 1967; *Brenguier et al.*, 2000; *Durkee et al.*, 2000b], satellite remote sensing [*Kaufman and Nakajima*, 1993; *Han et al.*, 1998; *Nakajima et al.*, 2001; *Breon et al.*, 2002; *Schwartz et al.*, 2002; *Schreier et al.*, 2006], surface-based remote sensing [*Feingold et al.*, 2003; *Kim et al.*, 2003], and all of the above [*Feingold et al.*, 2006]. The second type of indirect effect, first described by *Albrecht* [1989], addresses the dynamical response of the cloud resulting from an increase in aerosol concentration. In it, more numerous, smaller cloud droplets reduce droplet growth by collision and coalescence, and the consequent suppressed precipitation formation leads to enhanced cloud albedo. In this respect, in an early work, *Warner* [1968] attributed reduction in rainfall as a result of smoke particles from sugarcane fires; this effect has been confirmed in other observations [*Rosenfeld*, 1999]. There is less clear observational evidence concerning the response of total liquid water path (LWP) owing to the difficulty in isolating the aerosol effect from those arising from concurrent variations in meteorology. On the whole, there is limited observational support for the

[1]Department of Environmental Science and Engineering, California Institute of Technology, Pasadena, California, USA.
[2]Department of Atmospheric Sciences, University of Arizona, Tucson, Arizona, USA.
[3]Naval Postgraduate School, Monterey, California, USA.
[4]Department of Chemical Engineering, California Institute of Technology, Pasadena, California, USA.
[5]Departments of Chemical Engineering and Environmental Science and Engineering, California Institute of Technology, Pasadena, California, USA.

0148-0227/07/2006JD007985

second indirect effect [*Rosenfeld*, 2000; *Han et al.*, 2002; *Kaufman et al.*, 2005; *Rosenfeld et al.*, 2006; *Schreier et al.*, 2006]. With respect to marine stratocumulus, drizzle formation can exert a strong influence on cloud structure, thickness, and coverage [*Albrecht*, 1989; *Bretherton et al.*, 2004]. Variability in cloud droplet number concentration driven by variability in the number concentration of subcloud aerosol can lead to substantial variability in in-cloud drizzle characteristics. Drizzle formation can generate feedback to cloud dynamics such as decreasing boundary layer turbulence intensity and decreasing cloud top entrainment [*Stevens et al.*, 1998]. These drizzle-cloud dynamical interactions inevitably lead to changes in the cloud LWP, the sign and magnitude of which remain unclear.

[3] As noted above, strong observational support exists for the first indirect (Twomey) effect, although the quantitative relationship linking aerosol number concentration, N_a, in the accumulation mode [that in which the predominant number of cloud condensation nuclei (CCN) reside] and cloud droplet number concentration (CDNC) depends on aerosol concentration, size distribution, and composition, as well as meteorological conditions, such as updraft velocity. Once a perturbation occurs as a result of an increase in subcloud aerosol concentration, a series of cloud responses is induced, only the first of which is an increase in cloud droplet number activated. Cloud thickness and liquid water path, cloud top entrainment, and drizzle production can all be affected as a result of the initial perturbation, acting in concert to amplify or suppresses the original response of a brighter cloud. The moisture budget in cloud is determined by the balance between cloud top entrainment drying, surface evaporation, and cloud base drizzle rate. For example, *Stevens et al.* [1998] showed that with moist air above the boundary layer, drizzle formation actually leads to a higher LWP because the reduced cloud top entrainment drying exceeds the amount of direct cloud water loss by drizzle. On the basis of this result, in marine stratocumulus, an increase in subcloud aerosol leads to a decrease in LWP for a relatively dry free troposphere, whereas the opposite is predicted in a moist free troposphere [*Ackerman et al.*, 2004; *Lu and Seinfeld*, 2005]. A similar diverse trend in aerosol-induced cloud depth change, but under different criteria, is noted by Wood (Cancellation of aerosol indirect effects in marine stratocumulus through cloud thinning, submitted manuscript, 2006), such that on the timescale within a day, the aerosol induces a cloud-thickening effect if cloud base is low (<400 m), and a cloud-thinning effect if cloud base is high.

[4] Changes in subcloud aerosol also affect the cloud droplet size spectrum (the so-called dispersion effect) and thereby also the cloud albedo. *Liu and Daum* [2002] and *Peng and Lohmann* [2003] used cloud data from field studies and showed that the relative dispersion (which is defined as the ratio of the standard deviation to the mean radius of the cloud drop size distribution) apparently increased as cloud drop number concentration increased. Liu and Daum argued that the more numerous smaller droplets formed in a polluted cloud compete for water vapor and broaden the droplet size distribution compared with the unperturbed cloud. *Lu and Seinfeld* [2006] carried out detailed large-eddy simulations (LES) of marine stratocumulus with varying aerosol number concentrations under the same meteorological condition (sounding). On this basis, they found that cloud spectral relative dispersion actually decreases with increasing aerosol number concentration. This is explained by suppressed drizzle at increased aerosol loadings, which results in less spectral broadening by collision and coalescence processes, and more spectral narrowing by droplet condensational growth at the higher updraft velocities dynamically induced by suppressed drizzle. Thus, the actual direction of the spectral response resulting from an increase of aerosol depends on prevailing conditions.

[5] In this work, we report on a dedicated field experiment designed to probe aerosol-cloud relationships in clean and perturbed marine stratocumulus. The goal of the work is to provide a comprehensive set of data to evaluate aerosol indirect effects in marine stratocumulus. Section 2 describes the experiment. In section 3, we focus on a case study involving ship emissions. Section 4 is devoted to a statistical analysis of the ensemble of clouds sampled over the entire experiment.

2. Marine Stratus/Stratocumulus Experiment

[6] The Marine Stratus/Stratocumulus Experiment (MASE) field campaign was undertaken during July 2005 off the coast of Monterey, California. The goal of MASE was to make state-of-the-art measurements of aerosols and clouds in the climatically important regime of eastern Pacific marine stratocumulus clouds. The cold ocean surface, in combination with warm, dry air aloft, induces the formation of one of the world's most persistent stratocumulus cloud decks. The region of the Pacific atmosphere adjacent to the coast of California experiences air masses of very clean, background air as well as ones having strong anthropogenic influences. In addition, the prevalence of shipping lanes in this region offers the opportunity to study directly the effect of significant localized aerosol perturbations from ship emissions on marine stratocumulus properties, so-called ship tracks [*Coakley et al.*, 1987; *Durkee et al.*, 2000b, 2000c; *Schreier et al.*, 2006]. Indeed, ship emissions released below a stratocumulus deck provide a tailor-made realization of the indirect climatic effect of aerosols. The eastern Pacific region adjacent to the coast of California is, therefore, an ideal test bed for studying aerosol-cloud interactions. The July time frame was selected because it is the month during which the coverage of stratocumulus in this region is at its maximum. A total of 13 science flights were conducted between 2–17 July (Table 1). Measurements were carried out on board the Center for Interdisciplinary Remotely-Piloted Aircraft Studies (CIRPAS) Twin Otter aircraft during the mission. The instrumentation on board the Twin Otter is summarized in Table 2, and the data analysis process for the study is briefly described in the Appendix.

[7] Of the 13 Twin Otter flights that were conducted during MASE, six encountered strong, localized perturbations in aerosol concentration, size, and composition consistent with ship emissions. The subcloud aerosol and its impact on the stratocumulus layer were analyzed using a detailed aircraft cloud profiling strategy (Figure 1). Clear effects of enhanced aerosol loading in these cases were observed in cloud droplet concentration and droplet size distributions. The flight on July 5 (see Table 1) is selected

Table 1. Summary of Cloud Properties From Sampled Stratocumulus Clouds[a]

Case Name (Cloud Date)[b]	UTC Time, hh:mm	Cloud Base, m	Cloud Top, m	Cloud Base σ_w, m s^{-1}	N_a, cm^{-3}	CDNC, cm^{-3}	Cloud r_e, μm	Cloud LWC, g m^{-3}	Cloud LWP, g m^{-2}	Drizzle R_{CB}, mm day^{-1}	N_d, cm^{-3}	Cloud σ, μm	Cloud d	Cloud k
Cloud 2	20:39–22:20	315	555	0.18	1305 ± 340	228 ± 57	5.8 ± 0.7	0.09 ± 0.05	16.2	0.03 ± 0.04	0.06 ± 0.06	1.56 ± 0.22	0.35 ± 0.04	0.71 ± 0.05
							(6.0 ± 0.8)[c]	(0.09 ± 0.06)	(17.2)	(0.05 ± 0.05)		(1.58 ± 0.34)	(0.36 ± 0.04)	(0.68 ± 0.06)
Cloud 3	17:50–19:17	202	451	0.25	1068 ± 104	232 ± 64	5.6 ± 0.6	0.10 ± 0.05	18.0	0.03 ± 0.01	0.05 ± 0.04	1.43 ± 0.21	0.37 ± 0.05	0.66 ± 0.07
							(5.8 ± 0.7)	(0.10 ± 0.05)	(18.9)	(0.05 ± 0.02)		(1.47 ± 0.28)	(0.38 ± 0.05)	(0.62 ± 0.07)
Cloud 5A	17:21–18:55	222	667	0.29	401 ± 90	161 ± 40	8.1 ± 0.8	0.36 ± 0.08	92.4	0.46 ± 0.40	0.46 ± 0.15	1.69 ± 0.21	0.25 ± 0.02	0.84 ± 0.03
							(8.8 ± 0.9)	(0.42 ± 0.10)	(106)	(0.48 ± 0.39)		(1.96 ± 0.38)	(0.26 ± 0.03)	(0.77 ± 0.05)
Cloud 5B	18:55–20:25	222	732	0.25	384 ± 13	160 ± 42	7.5 ± 0.4	0.23 ± 0.5	66.4	0.12 ± 0.21	0.27 ± 0.06	1.64 ± 0.17	0.32 ± 0.03	0.75 ± 0.03
							(8.0 ± 0.5)	(0.25 ± 0.06)	(73.1)	(0.14 ± 0.21)		(1.74 ± 0.30)	(0.34 ± 0.04)	(0.68 ± 0.04)
Cloud 8	17:36–19:05	193	570	0.19	580 ± 162	118 ±32	9.2 ± 1.0	0.37 ± 0.08	85.5	0.22 ± 0.25	0.56 ± 0.48	1.91 ± 0.39	0.28 ± 0.05	0.78 ± 0.06
							(9.9 ± 1.7)	(0.41 ± 0.16)	(96.8)	(0.26 ± 0.31)		(2.04 ± 0.60)	(0.31 ± 0.06)	(0.71 ± 0.09)
Cloud 9	17:56–19:51	157	534	0.12	252 ± 32	70 ± 16	10.6 ± 1.0	0.35 ± 0.11	72.4	0.04 ± 0.09	0.37 ± 0.31	1.81 ± 0.47	0.24 ± 0.04	0.85 ± 0.04
							(11.1 ± 1.3)	(0.35 ± 0.15)	(71.3)	(0.05 ± 0.10)		(2.07 ± 0.88)	(0.26 ± 0.05)	(0.80 ± 0.06)
Cloud 10	18:10–19:57	300	685	0.06	72 ±5	43 ± 10	9.3 ± 0.8	0.09 ± 0.02	39.9	0.42 ± 0.37	0.11 ± 0.04	2.85 ± 0.43	0.40 ± 0.03	0.67 ± 0.04
							(9.5 ± 0.9)	(0.09 ± 0.02)	(48.6)	(0.69 ± 0.54)		(3.28 ± 0.85)	(0.41 ± 0.03)	(0.64 ± 0.05)
Cloud 13	17:46–19:46	101	450	0.17	827 ± 162	136 ± 48	7.3 ± 1.3	0.13 ± 0.08	41.7	0.27 ± 0.33	0.29 ± 0.21	2.21 ± 0.31	0.33 ± 0.05	0.71 ± 0.06
							(7.9 ± 1.7)	(0.15 ± 0.10)	(53.2)	(0.32 ± 0.37)		(2.42 ± 0.59)	(0.33 ± 0.08)	(0.63 ± 0.07)
Cloud 14A	17:53–19:03	67	364	0.11	780 ± 28	183 ± 31	7.7 ± 0.4	0.37 ± 0.03	52.2	0.33 ± 0.37	0.52 ± 0.16	2.14 ± 0.26	0.33 ± 0.02	0.71 ± 0.03
							(8.3 ± 0.7)	(0.41 ± 0.04)	(63.3)	(0.35 ± 0.37)		(2.40 ± 0.38)	(0.34 ± 0.03)	(0.63 ± 0.04)
Cloud 14B	19:06–20:26	115	371	0.17	687 ± 536	187 ± 39	8.4 ± 0.6	0.38 ± 0.04	54.1	0.40 ± 0.36	0.75 ± 0.22	2.34 ± 0.32	0.35 ± 0.02	0.67 ± 0.03
							(9.3 ± 0.8)	(0.44 ± 0.05)	(66.1)	(0.48 ± 0.39)		(2.55 ± 0.48)	(0.37 ± 0.02)	(0.59 ± 0.04)
Cloud 15	20:03–20:54	88	370	N/A	447 ± 332	289 ± 27	5.7 ± 0.7	0.19 ± 0.03	53.7	0.04 ± 0.03	0.09 ± 0.04	1.49 ± 0.12	0.20 ± 0.03	0.89 ± 0.04
							(6.1 ± 1.1)	(0.19 ± 0.03)	(55.6)	(0.08 ± 0.05)		(1.55 ± 0.15)	(0.20 ± 0.05)	(0.87 ± 0.05)
Cloud 16	20:49–21:28	100	366	N/A	479 ± 24	232 ± 34	7.5 ± 0.5	0.30 ± 0.04	52.9	0.13 ± 0.11	0.42 ± 0.09	1.91 ± 0.27	0.30 ± 0.02	0.75 ± 0.03
							(7.9 ± 0.6)	(0.32 ± 0.05)	(58.8)	(0.19 ± 0.11)		(2.09 ± 0.34)	(0.31 ± 0.03)	(0.68 ± 0.04)
Cloud 17	19:24–20:33	85	268	0.16	490 ± 606	289 ± 35	6.5 ± 0.5	0.27 ± 0.05	33.0	0.02 ± 0.03	0.09 ± 0.04	1.41 ± 0.16	0.25 ± 0.02	0.83 ± 0.03
							(6.6 ± 0.5)	(0.28 ± 0.05)	(34.6)	(0.04 ± 0.04)		(1.43 ± 0.16)	(0.26 ± 0.03)	(0.81 ± 0.04)

[a]See Appendix for the calculation.
[b]Case is named based on the date in July 2005. A and B refer to the first and second cloud sampled on that day if more than one.
[c]Value in the parentheses is integrated over the combined cloud and drizzle spectrum.

Table 2. Aerosol and Cloud Instrument Payload on Twin Otter During MASE

Parameter	Instrument	Averaging Time	Detection Limit	Size Range Detected
Particle Number Concentration	Condensation Particle Counter (TSI CPC 3010)	1 s	0–10,000 particles cm^{-3}	D_p >10 nm
Particle Number Concentration (Including Ultrafine)	Condensation Particle Counter (TSI CPC 3025)[a]	1 s	0–100,000 particles cm^{-3}	D_p >3 nm
Aerosol Size Distributions at Dry and Humid Conditions	Scanning differential mobility analyzer (Dual Automated Classified Aerosol Detector, DACAD)	73 s	N/A	10–700 nm
Aerosol Size Distribution	Passive Cavity Aerosol Spectrometer Probe (PCASP)	1 s	N/A	0.1–2.6 μm
Separation of Cloud Droplets From Interstitial Aerosol	Counterflow Virtual Impactor	N/A	N/A	N/A
Cloud Droplet Size Distribution	Phase Doppler Interferometer (PDI)	1 s	N/A	4–200 μm
Cloud and Drizzle Drop Size Distribution	Cloud, Aerosol, and Precipitation Spectrometer (CAPS)[b]	1 s	N/A	0.4 μm–1.6 mm
Cloud Droplet Size distribution	Forward Scattering Spectrometer Probe (FSSP)	1 s	N/A	1–46 μm
Cloud Droplet Liquid Water Content	Light diffraction (Gerber PVM-100 probe)	1 s	N/A	~5–50 μm
Aerosol Bulk Ionic Composition and Soluble Organic Composition	Particle-into-Liquid Sampler (PILS)	5 min	0.02–0.28 $\mu g\ m^{-3}$ (depending on species)	<1 μm
Aerosol Bulk Composition (Nonrefractory Species)	Aerodyne Time-of-Flight Aerosol Mass Spectrometer (TOF-AMS)	1 s or 15 s	<0.25 $\mu g\ m^{-3}$ (all species)	D_{va} ~40 nm–1 μm
Soot Absorption	Photoacoustic Absorption Spectrometer (PAS)	1 s	1 Mm^{-1}	10 nm–5 μm
Soot Absorption	Particle Soot Absorption Photometer (PSAP)	1 s or higher	N/A	N/A

[a]The ultrafine CPC, referred to UFCPC in the text.
[b]Drizzle drop size distribution is measured by the cloud imaging probe (CIP) included in the CAPS package.

as a case study because of the particularly pronounced effect of ship emissions.

[8] The MASE experiment was undertaken to address following scientific questions:

[9] (1) Does cloud droplet number concentration increase in response to increasing subcloud aerosol amount? And, is cloud droplet size reduced?

[10] (2) Is the drizzle rate suppressed owing to more numerous cloud droplets? Furthermore, does the cloud liquid water path or averaged liquid water content increase because of drizzle inhibition?

[11] (3) Do we observe an aerosol-induced droplet spectral dispersion effect?

[12] Table 3 lists key questions concerning aerosol indirect effects on marine stratocumulus that have been addressed previously by in situ measurements and LES simulations.

3. Case Study: Ship Tracks on July 5, 2005

3.1. Case Description

[13] The region observed on July 5 (denoted cloud 5A in Table 1), sampled over 17:30–19:00 UTC (local time = UTC − 7h), is selected for a detailed case study. Measurements of both aerosol number concentration and composition indicate this region was impacted by ship emissions. Aerosol chemistry measurements, comprising the Aerodyne Time-of-Flight Aerosol Mass Spectrometer (TOF-AMS) (flown for the first time during MASE), the Particle-into-Liquid Spectrometer (PILS), and the Photoacoustic Absorption Spectrometer (from which black carbon concentration is inferred) (Table 2), showed a number of significant features: (1) a fairly concentrated layer of organic carbon aerosol (~3 $\mu g\ m^{-3}$) overlaid the marine boundary layer (MBL); (2) within the MBL, organic aerosol loading was lower (~0.5 $\mu g\ m^{-3}$); however, sulfate aerosol loading was comparable to that overlying the MBL; (3) the ship tracks are associated with a strong enhancement in MBL sulfate aerosol (~0.5 to 2 $\mu g\ m^{-3}$) above the background but with virtually no observable enhancement in organic or black carbon aerosol.

[14] Extensive horizontal legs flown through the ambient cloud and ship tracks provide fine-scale (~1 Hz or 50-m resolution) three-dimensional data on the cloud properties. Long flight legs of ~30 km enabled sufficient averaging to reduce sampling uncertainty and provided insights into the spatial variability at each flight level. We study the impacts of aerosol on the cloud properties at the fine scale by

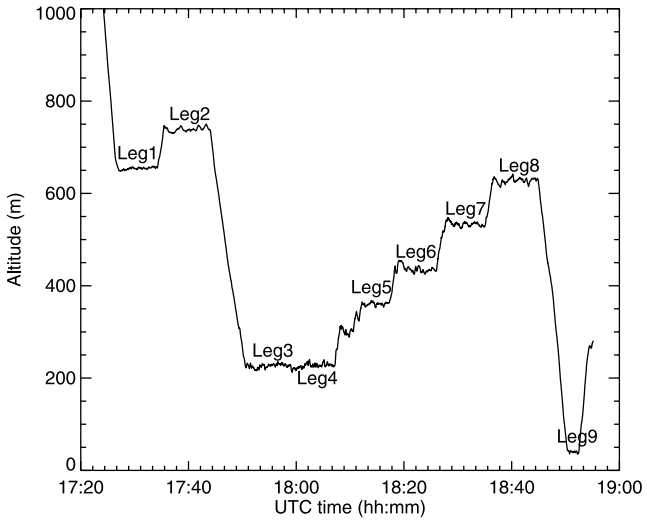

Figure 1. Time series of aircraft altitude for cloud 5A in Table 1 (5 July 2005). Each horizontal-level leg is labeled.

Table 3. Indirect Effects on Marine Stratocumulus

	In Situ Aircraft Observations	LES or ERM[a] Simulations
	Twomey effect	
CDNC increases due to N_a increase	*Ferek et al.* [1998]; *Taylor et al.* [2000] of MAST; *Brenguier et al.* [2000] of ACE2; *Feingold et al.* [2006]; this study	*Feingold et al.* [1994]; *Kogan et al.* [1996; 1997]; *Jiang et al.* [2001; 2002]; *Ackerman et al.* [2004]; *Lu and Seinfeld* [2005]; this study
Smaller droplet size due to CDNC increases	*Hudson and Yum* [1997] of FIRE and ASTEX; *Taylor et al.* [2000] of MAST; *Brenguier et al.* [2000] of ACE2; *Feingold et al.* [2006]; this study	*Feingold et al.* [1994]; *Kogan et al.* [1996; 1997]; *Jiang et al.* [2001; 2002]; *Lu and Seinfeld* [2005]; this study
	Second Indirect Effect	
Drizzle suppression due to higher CDNC (Albrecht effect)		
Fewer drizzle drops	*Ferek et al.* [1998]; *Ferek et al.* [2000] of MAST; this study	This study
Smaller drizzle rate	*Ferek et al.* [2000] of MAST; this study	*Jiang et al.* [2001; 2002]; *Ackerman et al.* [2004]; *Lu and Seinfeld* [2005]; this study
Column LWP or local LWC responses due to drizzle suppression		
LWP/LWC increase	*Taylor et al.* [2000] of MAST[b]; this study of the ship track impacted cloud	*Jiang et al.* [2001, 2002]; *Ackerman et al.* [2004] for ASTEX, FIRE (CDNC < 225 cm^{-3})[c] and DYCOMS-II (CDNC < 35 cm^{-3})[c]; *Lu and Seinfeld* [2005] for ASTEX; this study of the ship track impacted cloud
LWP/LWC decrease	*Ferek et al.* [2000] of MAST; this study of the overall 13 clouds sampled	*Feingold et al.* [1997]; *Ackerman et al.* [2004] for FIRE (CDNC > 225 cm^{-3})[c] and DYCOMS-II (CDNC > 35 cm^{-3})[c]; *Lu and Seinfeld* [2005] for FIRE
Entrainment rate increases	None	*Ackerman et al.* [2004]; *Lu and Seinfeld* [2005]
Cloud cover increases due to drizzle suppression	None[d]	*Ackerman et al.* [2003]
Lifetime increases due to drizzle suppression	None	None
	Dispersion effect	
Narrower droplet spectral width due to higher CDNC or N_a	*Hudson and Yum* [1997] of FIRE and ASTEX; *Miles et al.* [2000][e]; in-flight data for all clouds and flight-averaged data for clouds with CDNC > 100 cm^{-3} in *Pawlowska et al.* [2006]; this study of the ship track impacted cloud	*Feingold et al.* [1997]; *Lu and Seinfeld* [2006]; this study
Decrease or increase of relative dispersion due to higher CDNC or N_a		
Relative dispersion decrease	*Miles et al.* [2000][e]; in-flight data for all clouds in *Pawlowska et al.* [2006]; this study of the ship track impacted cloud	*Feingold et al.* [1997]; *Lu and Seinfeld* [2006]; this study
Relative dispersion increase	*Liu and Daum* [2002]; Flight-averaged clouds in *Pawlowska et al.* [2006]; this study of the overall 13 clouds sampled (on the basis of N_a)	None

[a]Eddy resolving model is a 2D version LES.
[b]Drizzle occurrence was inferred by satellite, and LWP is from microwave radiometer.
[c]Or the threshold of surface drizzle rate of 0.1 mm day^{-1}.
[d]This effect is difficult to measure by aircraft and is mostly seen in satellite studies, e.g., *Kaufman et al.* [2005] and *Rosenfeld et al.* [2006].
[e]Compiled database of "marine" and "continental" low clouds. We assume that "continental" clouds are more polluted than marine clouds.

comparing data in the ship track regions against those in the adjacent unperturbed clouds. The aircraft flew through an extensive region of stratocumulus cloud features with several cloud rolls. The flight path is shown against the satellite imagery (Figure 2) from the Geostationary Operational Environmental Satellite (GOES) visible channel (channel 1, 0.65 μm). The cloud rolls were aligned approximately parallel to the mean wind. The ship tracks are most apparent in the GOES near-infrared (IR) channel (channel 2, centered at 3.9 μm, Figure 3). Because liquid water at this wavelength is moderately absorbing, sunlight does not penetrate the cloud deeper than about 100 m, so that the cloud albedo depends mainly on the cloud droplet size in the upper region of the cloud. The near-IR imagery reveals two marked brighter (high reflectance) narrow, curvilinear cloud lines in the sampling period. Between and outside the two brighter ship track impacted clouds are darker regions that are still cloudy from the visible channel picture. The ship track on the west was sampled with nine horizontal traverses (Figure 1), seven through the cloud layers and two above and below clouds, respectively. The horizontal flight legs are numbered based on the time sequence.

3.2. SubCloud Aerosol Number Concentration

[15] The flight path delineated according to the magnitude of aerosol and cloud droplet number concentrations is presented in Figure 4. The horizontal distance (X) includes a shift by the mean horizontal wind so that the spatially coincident structures of aerosol and cloud drop number concentrations (i.e., near- or below-cloud base aerosol number concentration versus cloud droplet number concentration) are revealed. A noticeable peak (orange to red color)

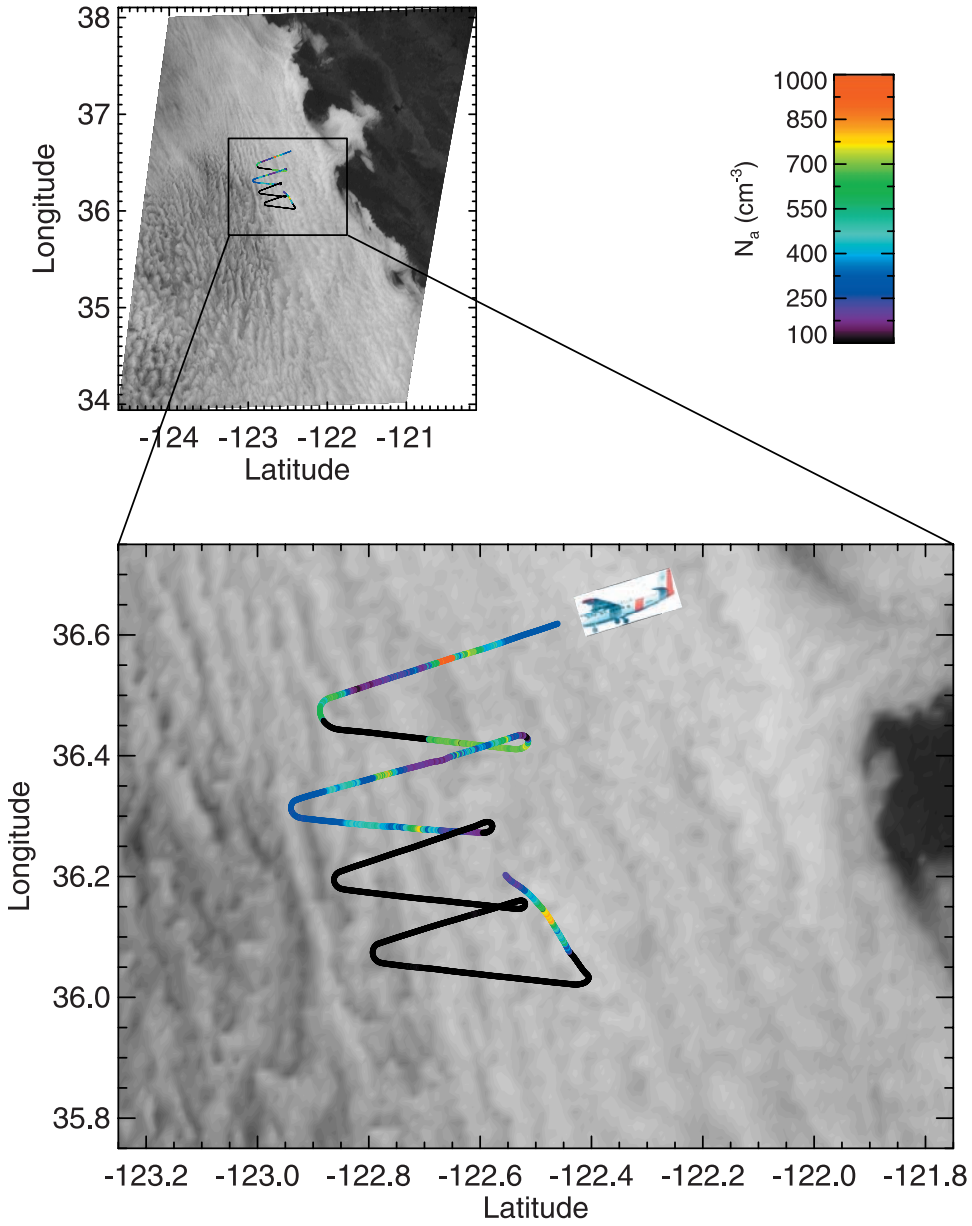

Figure 2. GOES-10 Band 1 (shortwave, centered at 0.65 μm) satellite picture at 17:45 UTC, 5 July 2005. The horizontal resolution of this band is 1 km. GOES data are obtained from the National Oceanic and Atmospheric Administration (NOAA) Satellite and Information Service. Flight path is colored according to aerosol number concentration measured by CPC.

in aerosol number concentration located around $X = 59$ km is shown below and above cloud (Figure 4a), which is coherent with the apparent peak in cloud drop number concentration in the same location (Figure 4b). Figure 4c shows clearly that the horizontal distribution of cloud droplet number concentration varies with the horizontal distribution of below-cloud aerosol number concentration. Both Condensation Particle Counter (CPC) and Ultrafine CPC (UFCPC) data exhibit covariabilities with cloud droplet number concentration. The difference between data from the UFCPC and the CPC instruments represents the number concentration of ultrafine particles between 3 and 12 nm diameter; this indicates that freshly nucleated particles in the Aitken mode are significant in the major ship track region. Another smaller peak in CPC and UFCPC located around $X = 48 - 54$ km is also seen at a similar X location in the cloud drop number concentration data. The spatially coherent peaks in aerosol and cloud number concentrations and the narrow curvilinear cloud lines on the satellite imagery suggest that increases of cloud droplet number concentration are associated with and can be ascribed to increases in below-cloud CCN concentration by particles emitted or formed from ship effluent.

[16] The relationship between cloud droplet number concentration, CDNC, and subcloud aerosol number concentration, N_a, is shown in Figure 5. Although the spatial distributions of UFCPC and CPC data measured below cloud visually match the patterns of cloud drop number concentration in the middle to upper cloud (Figure 4), some mismatches do exist. This is because the below-cloud and

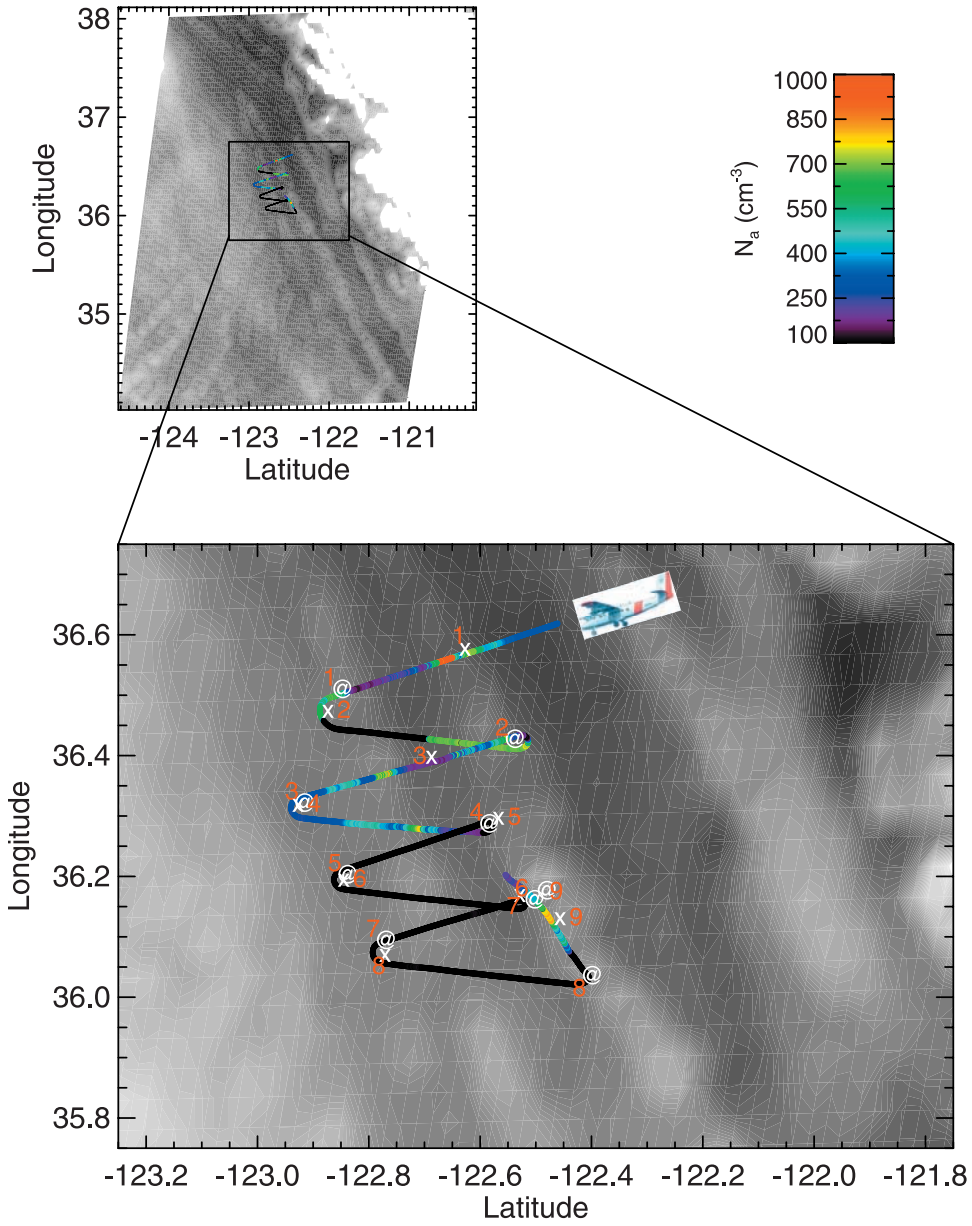

Figure 3. GOES-10 satellite Band 2 (centered at 3.9 μm) satellite picture at 17:45 UTC, 5 July 2005. The horizontal resolution for this band is 4 km. GOES data are obtained from NOAA Satellite and Information Service. Flight path is colored according to aerosol number concentration measured by CPC. Horizontal legs are marked on the path (×, start; @, end).

the middle-to-upper cloud measurements were not carried out simultaneously. The satellite imagery (Figure 3) shows a somewhat broadened line feature in the downstream direction (relative to the northwest mean wind). Meanwhile, the CDNC measurement carried out at the later mission time than the subcloud aerosol measurement (Figure 4) also shows a wider CDNC peak at about X = 48 – 56 km, as compared with the peaks in the CPC and UFCPC data at the similar horizontal location. The wider peak in CDNC is a result of the dispersion of the ship plume from its source. Therefore those CDNC data showing some widening and mismatch with upstream subcloud aerosol data are removed from the regression calculation (Figure 5). The regression results (Figure 5b) suggest that CDNC is highly positively correlated with N_a over a wide range of N_a, while the corresponding meteorological condition is about constant.

3.3. Cloud and Drizzle

[17] Figure 6 shows the cloud droplet number concentration on each horizontal flight leg. The cloud droplet number distribution exhibits some wave-like structures with several apparent peaks through four horizontal traverses (legs 1, 5, 6, 7, and 8) and more random distribution at legs near cloud base (legs 3 and 4, not shown), probably because the airplane penetrated in and out of cloud base. The width of the major peak is about 5 km (X = 56 – 61 km); the total width of the ship track that includes several wave-like structures is about 21 km (X = 44 – 65 km). (From the Monterey Area Ship Track Experiment

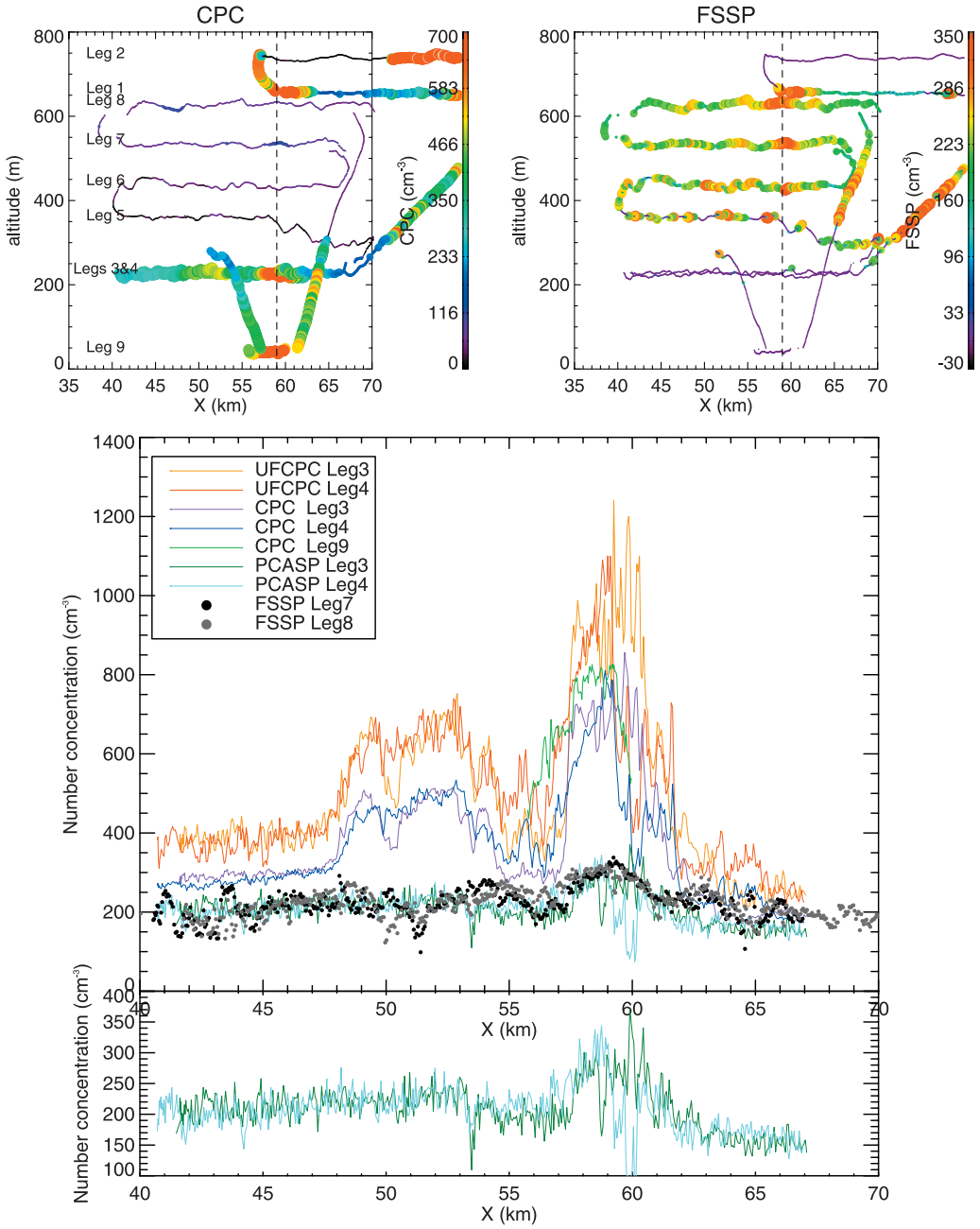

Figure 4. Flight paths colored according to aerosol number concentrations (upper left) and cloud drop number concentrations (upper right). The flight path has been shifted horizontally by the wind drift so that the vertical profiles can be aligned. The lower panel shows the below or near cloud base aerosol number concentrations from the Passive Cavity Aerosol Spectrometer Probe (PCASP), CPC, and UFCPC, and cloud droplet number concentrations in the middle to upper regions of the stratocumulus cloud from FSSP. The PCASP data are masked by the FSSP data so as to be separately plotted at the bottom. The east direction is on the right hand side of each plot.

(MAST), averaged ship track widths were about 9 ± 5 km [*Durkee et al.*, 2000a]). Outside this broad ship track region, lower cloud droplet number concentrations exist (denoted "Clean west" and "Clean east" in the figure), which are considered to be clean, undisturbed regions. These three cloud regions have about the same cloud depth, facilitating the study of the aerosol indirect effect at essentially constant cloud depth.

[18] Cloud properties along two horizontal leg flights in the upper regions of the cloud through the solid stratocumulus deck are now explored (legs 7 and 8 in Figures 7 and 8, respectively). Averaged cloud properties in two unperturbed regions and the ship track region shown in Figure 6 are also given in Table 4. Although the horizontal distribution of cloud liquid water content (LWC) seems in phase with that of CDNC in Figures 7 and 8, carefully averaging the cloud LWC over the ship track and clean

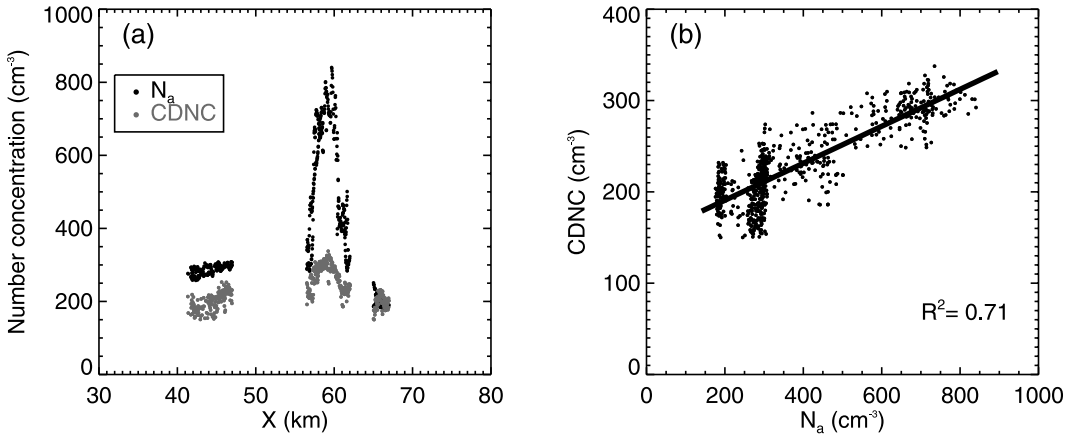

Figure 5. Below-cloud aerosol number concentration and cloud droplet number concentration. (a) Aerosol data are from legs 3 and 4, and cloud data are from legs 7 and 8 as shown in Figure 4 with some data points removed for better linear regression (line) shown in Figure 5b.

regions, respectively, shows a higher cloud LWC in the ship track than the clean regions for both legs (Table 4). The averaged drizzle drop number concentration (N_d) is lower in the ship track than the clean regions for both legs. The drizzle LWC is higher in the ship track region for leg 7 but lower in the ship track region for leg 8. For both legs, the drizzle rate is higher in the ship track region.

[19] In sum, we see cloud LWC at the upper portion of the cloud increased in the ship track region because of drizzle suppression as reflected by drizzle drop number concentration. We also note that this selected cloud case (cloud 5A) is one of the most strongly drizzling clouds (cloud base drizzle rate $\sim$0.5 mm day^{-1}) among all those sampled.

3.4. Cloud Drop Spectral Dispersion

[20] As noted in section 1, changes in subcloud aerosol number concentration can affect the shape of the cloud drop size distribution, the so-called dispersion effect, influencing cloud albedo. Cloud droplet effective radius (r_e) is a key parameter that links cloud microphysics with cloud optical properties in large-scale models [*Slingo and Schrecker*, 1982]. Parameterization of r_e is generally represented through the parameter k, defined by

$$k = \frac{r_v^3}{r_e^3}. \tag{1}$$

where r_v is the volume mean radius of the cloud droplet size distribution. By the definition that $r_v = (3\mathrm{LWC}/4\pi\rho_w \mathrm{CDNC})^{1/3}$, where ρ_w is the density of water,

$$r_e = \left(\frac{4}{3}\pi\rho_w\right)^{-1/3} k^{-1/3}\mathrm{LWC}^{1/3}\mathrm{CDNC}^{-1/3}. \tag{2}$$

The coefficient k can be expressed analytically as a function of droplet relative dispersion, $d = \sigma/r_m$, as [*Lu and Seinfeld*, 2006]

$$k = \frac{(1+d^2)^3}{(sd^3+1+3d^2)^2}. \tag{3}$$

where σ is the standard deviation (or cloud drop spectral width), r_m is the mean radius of the droplet distribution, and s is the skewness of the drop spectrum, generally assumed to be zero.

[21] Through the relationship between k and d, cloud spectral shape affects cloud optical properties. *Liu and Daum* [2002] suggested that an increase in aerosol number concentration would lead to an increase in relative dispersion and a cloud darkening. In their work, not all cloud cases show the suggested increasing trend of d as a result of pollution. The polluted and clean cloud cases were not necessarily subject to identical meteorological soundings and may have experienced various updraft velocities. By contrast, on the basis of LES simulations assuming a constant meteorological condition but varying only aerosol number concentration, *Lu and Seinfeld* [2006] demonstrated that stratocumulus cloud would evidence the opposite effect, namely, a decrease in relative dispersion and a consequent cloud brightening.

[22] Patterns in Figures 7 and 8 reveal interesting spatial correlations of several variables with cloud droplet number concentration. For example, the horizontal distributions of d and σ are out of phase with that of CDNC, while the parameter k approximately varies directly with CDNC. The relationship between relative dispersion and CDNC displayed in Figure 9 for both cloud and cloud-and-drizzle (referred to as combined cloud and drizzle spectra, hereafter) is more pronounced for leg 7 than for leg 8 but is still discernable for leg 8; similar results hold for the relationship between k and CDNC. The value of k is about 10% smaller when drizzle drops are taken into account. The value of k is found to depend inversely on relative dispersion because spectral skewness (s) is generally less than unity as shown in Table 4. Averaged dispersion effects in ship track and clean regions show that the former features smaller d and σ and larger k than its cleaner counterpart for legs 7 and 8; this is also the case when the drizzle size distribution is taken into account in calculating d, σ, and k.

[23] The range of values of sampled r_m, σ, and d in legs 7 and 8 (Figures 7, 8, and 9) are generally in agreement with those reported from several stratocumulus clouds in the Second Aerosol Characterization Experiment (ACE2) shown

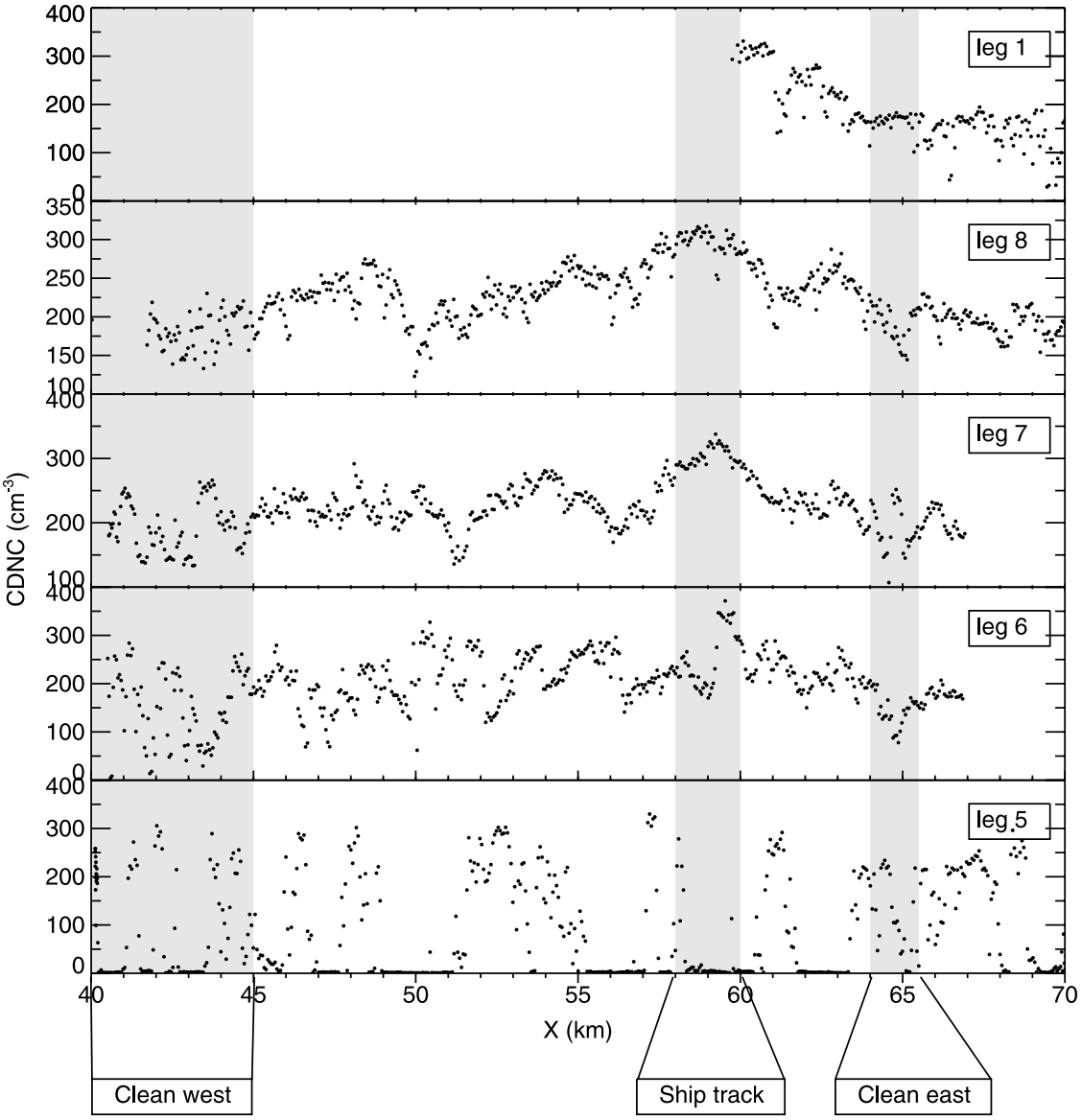

Figure 6. Cloud droplet number concentration distribution at each horizontal leg for the first cloud sampled on 5 July 2005. Vertical panels are arranged according to the mean altitude (numbers are shown for each leg) of each leg denoted in the legend. Each panel has been shifted horizontally by the wind drift for better alignment of ship track and the relatively cleaner regions. The shaded areas define the "Clean west", "Ship track", and "Clean east" regions used in later analysis shown in Table 4.

in Figure 1 (line) of *Pawlowska et al.* [2006] compared at the same range of CDNC. Furthermore, the fine-scale inverse relationships r_m-CDNC, σ-CDNC, and d-CDNC sampled in horizontal legs 7 and 8 (scale ~50 m) are consistent with in-flight results (scale ~10 m) from ACE2. Pawlowska et al. assumed no in-flight horizontal variability of aerosol and attributed the in-flight observations of the decrease of σ and d with CDNC to the variability of cloud base updraft velocity. However, because of negligible variations in the cloud base updraft between ship track and clean regions, the MASE in-flight relationships of r_m-CDNC, σ-CDNC, and d-CDNC can be attributed to the subcloud aerosol number concentration. Therefore given the strong correlation of subcloud aerosol number concentration with CDNC (Figure 5), we illustrate the possible dependence of r_m (inverse), σ (inverse), d (inverse), and k (direct) on subcloud aerosol number concentration. The relationships σ-N_a, d-N_a, k-N_a, and k-d also agree with those derived from the LES studies by *Lu and Seinfeld* [2006]. We will return to the dependence of d on CDNC at the "ensemble cloud scale" from all clouds sampled in MASE in Section 4.

3.5. Case Study Summary

[24] In summary, the upper region of the ship track-influenced cloud is characterized by higher cloud droplet number concentration, smaller relative dispersion, larger k, fewer drizzle drops, smaller cloud mean radius, and narrower cloud drop spectral width. Drizzle suppression by the ship track effluent is identified, which shows a lower drizzle drop

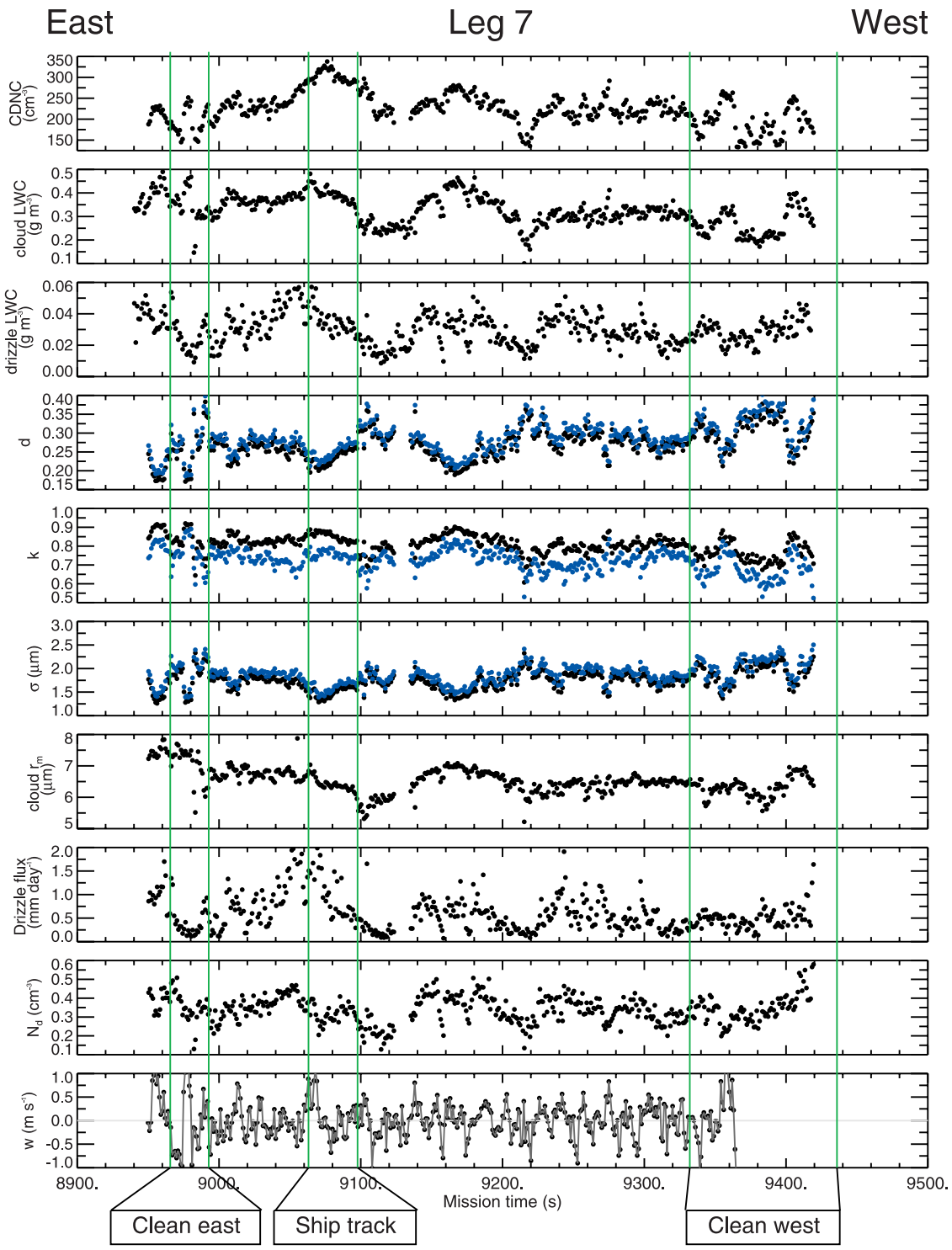

Figure 7. Time series of cloud and drizzle properties for horizontal leg 7. The ship track and two clean regions are labeled. Blue points are those calculated over the cloud-and-drizzle spectra.

number concentration in the ship track region. This likely leads to a higher upper cloud LWC in the ship track region.

4. Ensemble-Averaged Clouds Sampled in MASE

[25] Ensemble scale (~several tens of kilometers; i.e., by averaging data along horizontal legs) impacts of subcloud aerosol on cloud properties are now explored. Specifically, we address the relationships of cloud droplet number concentration, cloud effective radius, drizzle rate, cloud LWP, and relative dispersion on subcloud aerosol number concentration. We select 13 sampled clouds from the set of MASE flights for analysis. The clouds exhibit a wide range of subcloud aerosol number concentrations, from 70 to 1300 cm^{-3}, where in some cases ship tracks were present. Cloud base and top also show some degree of variation

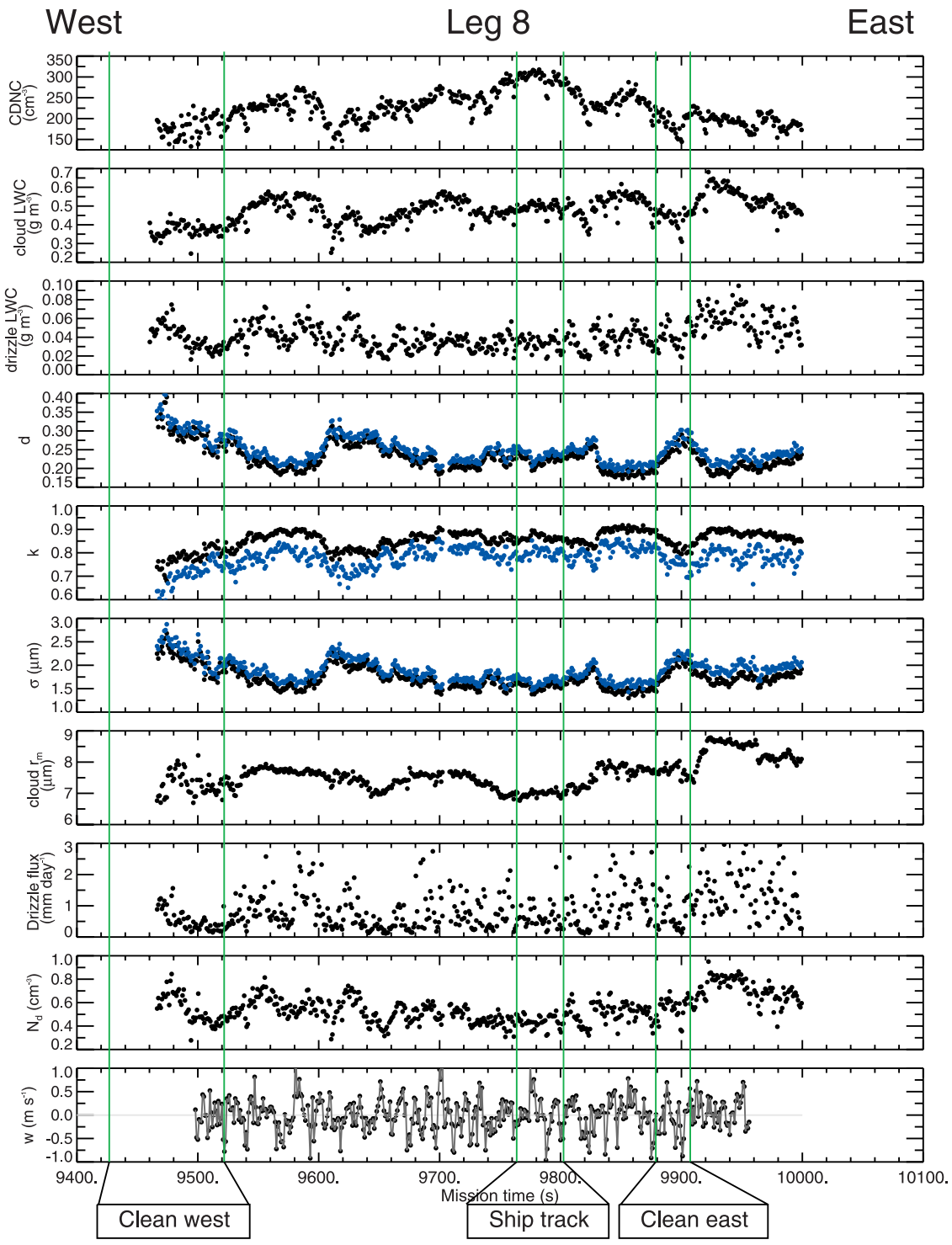

Figure 8. Similar to Figure 7 but for horizontal leg 8.

among cases. This offers an opportunity to study aerosol impacts on cloud microphysics and dynamics under a broad range of conditions. Table 1 summarizes properties of the MASE clouds studied.

4.1. Ensemble-Averaged Cloud and Aerosol Number Concentration

[26] The number of cloud droplets formed is controlled principally by the number of CCN at cloud base and vertical velocity. We determine the subcloud aerosol number concentration by averaging the measured aerosol number concentration within about 100 m below cloud base. The vertical distribution of aerosol number concentration below cloud base is more or less uniform if the cloud is not decoupled from the surface or the aerosol is not influenced by ship emissions. In ship track regions, the subcloud aerosol consists of a mixture of ambient marine aerosol and ship emissions. Nevertheless, the chemical composition

Table 4. Summary of the Averaged Cloud Properties Sampled in (a) Leg 7 and (b) Leg 8 for the Ship Track Region and the Neighboring Relatively Cleaner Regions[a]

Region	CDNC, cm^{-3}	cloud LWC, g m^{-3}	drizzle LWC, g L^{-1}	cloud d,	cloud k,	F_{drz}, mm day^{-1}	N_d, cm^{-3}	cloud r_m, μm	drizzle r_m, μm	cloud r_e, μm	cloud σ, μm	cloud s,
						(a) Leg 7						
Clean West	176	0.25	31	0.32 (0.34)[b]	0.74 (0.64)	0.50	0.36	6.26	25.2	7.65	2.00 (2.14)	0.12 (1.28)
Clean East	172	0.32	27	0.28 (0.30)	0.80 (0.73)	0.45	0.36	7.01	23.8	8.19	1.96 (2.09)	−0.26 (0.85)
Ship Track	303	0.39	35	0.23 (0.25)	0.85 (0.75)	1.07	0.32	6.40	25.4	7.13	1.49 (1.60)	−0.20 (2.48)
						(b) Leg 8						
Clean West	179	0.37	39	0.29 (0.31)	0.78 (0.70)	0.54	0.55	7.30	23.9	8.63	2.12 (2.27)	−0.15 (0.84)
Clean East	190	0.44	41	0.25 (0.27)	0.84 (0.76)	0.79	0.56	7.72	23.5	8.71	1.90 (2.06)	−0.37 (1.18)
Ship Track	300	0.50	34	0.22 (0.24)	0.87 (0.80)	0.88	0.45	6.98	23.5	7.69	1.54 (1.66)	−0.35 (1.50)

[a]See Figure 6, source for definitions of the regions.
[b]Value in the parenthesis is integrated over the combined cloud and drizzle spectrum.

of the subcloud aerosol composition for all MASE clouds is basically dominated by ammonium bisulfate, $(NH_4)HSO_4$. The subcloud dry aerosol size distributions do not show significant variations in shape among all clouds, and they can be approximately characterized by two evident modes with mode radius around 25 nm and 100 nm. Measured vertical distributions of cloud droplet number concentrations tend to be roughly constant in the broad middle portion of the cloud with smaller values near cloud top and base owing to cloud-clear air interfacial mixing. Some cases, for example that on 5 July, which exhibited a constant CDNC in a narrower middle region of the cloud, also exhibited much smaller CDNC concentration in the lower portion of the cloud, which could be associated with scattered cumulus below the well-mixed stratocumulus. The ensemble average of aircraft sampled data for each case shows a direct dependence of CDNC on subcloud aerosol number concentration, as expected (Figure 10). This relationship can be approximately represented with the power law function shown in Figure 10. The correlation is improved when cloud base updraft velocity variability (using σ_w, see Table 1) is taken into account,

$$\log \mathrm{CDNC} = 1.176 + 0.458 \ \log \ N_a + 0.315 \log \sigma_w, \quad (R^2 = 0.72). \tag{4}$$

Results from observations of stratocumulus by *Martin et al.* [1994] are also displayed in the figure, where the clouds were sampled over the eastern Pacific Ocean near California, South Atlantic, sea around the British Isles, and North Atlantic near Azores.

4.2. Ensemble-Averaged Cloud Drop Effective Radius

[27] Cloud radiative properties, e.g., cloud optical depth and albedo, are most influential near cloud top; therefore, r_e shown in Table 1 is calculated by averaging observations

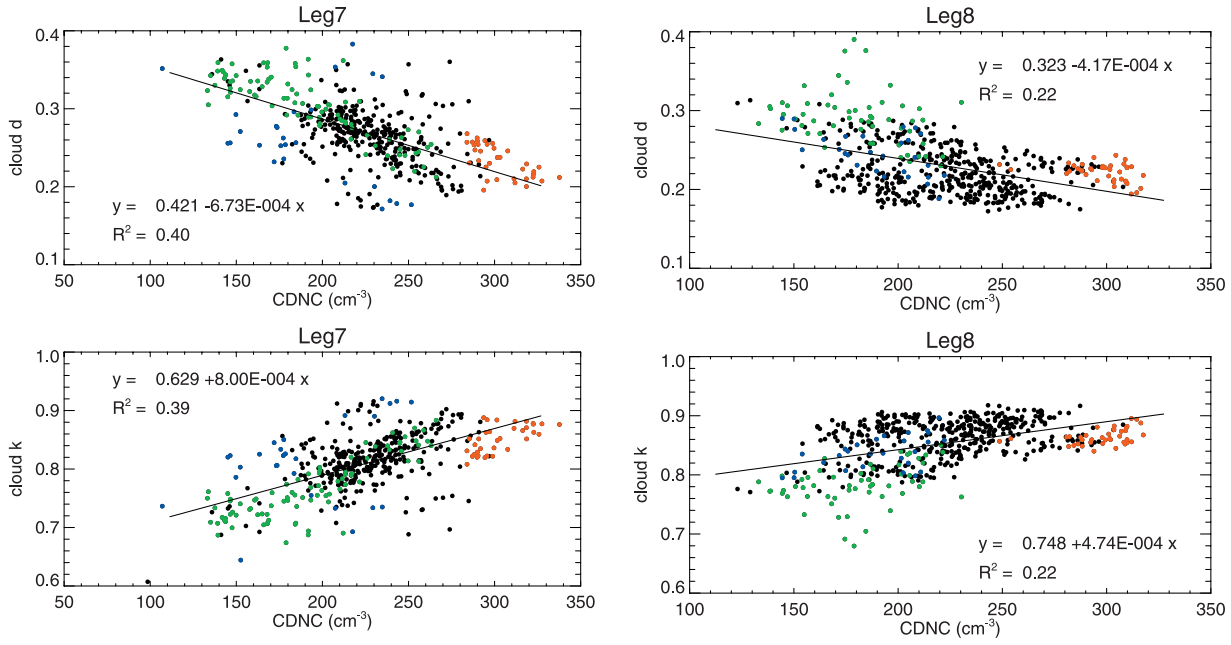

Figure 9. Correlation of relative dispersion (upper) and coefficient k (lower) with cloud drop number concentration along the horizontal leg 7 (left column) and leg 8 (right column). Data points are calculated over the cloud spectrum. Clean and ship track regions defined as in Figures 7 and 8 are marked with different colors: "Clean west" (green), "Clean east" (blue), and "Ship track" (red). Linear regression results are also shown.

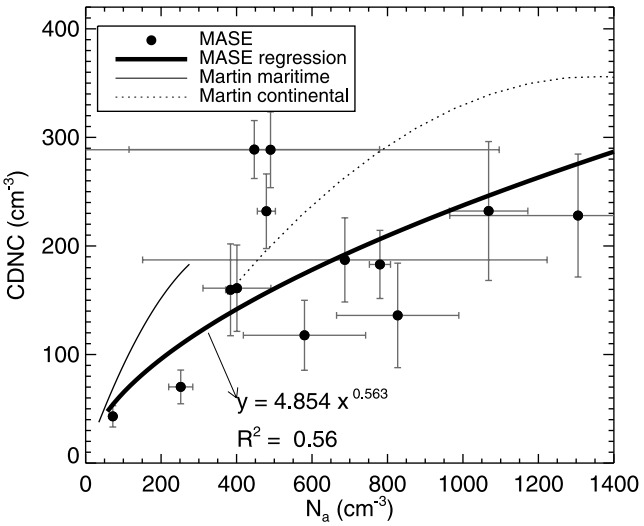

Figure 10. Relationship between cloud droplet number concentration and below-cloud aerosol number concentration. Error bar represents the standard deviation about the mean. Values are from Table 1. The thick solid line is the power law fit to the data. The thin solid and dotted lines are from *Martin et al.* [1994] for maritime and continental stratocumuli, respectively.

over the upper third of the cloud depth. The effective radius integrated over the cloud-and-drizzle spectrum is larger than that integrated over the cloud spectrum by about 0.1 to 0.9 μm; the difference is approximately proportional to the drizzle drop number concentration. Figure 11 shows clearly the decreasing trend of cloud droplet effective radius with increasing cloud droplet number concentration and sub-cloud aerosol number concentration for all 13 clouds. These trends continue to hold when the combined cloud and drizzle effective radius is used (not shown). We further group the data based on the cloud LWP. Figure 11 shows that the expected inverse relationship between r_e and CDNC is still strong for each LWP category. Therefore the overall feature of the MASE clouds is a smaller effective radius in more polluted clouds at the same LWP, a clear demonstration of the first indirect effect.

4.3. Ensemble-Averaged Drizzle

[28] Drizzle is common in the MBL [e.g., *van Zanten et al.*, 2005; *Wood*, 2005a] and plays a vital role in the evolution of stratocumulus [*Paluch and Lenschow*, 1991]. Basic considerations suggest that the modulation of drizzle by changes in anthropogenic aerosol number concentration can regulate cloud amount and thickness [*Albrecht*, 1989; *Pincus and Baker*, 1994]. Drizzle drop number concentrations (N_d) measured during MASE, with average values in the range of 0.05–0.5 cm^{-3}, are given in Table 1.

[29] The measured vertical profile of drizzle number concentration increases roughly linearly with height in the cloud and reaches a maximum value near cloud top for 11 out of 13 clouds sampled (not shown). The vertical profile of drizzle drop mean radius increases asymptotically with decreasing height, and the largest drizzle drops occur near or below cloud base. The maximum value of N_d near cloud top, together with the smallest drizzle drop mean size, largest cloud droplet size, and spectral distribution, suggests that the drizzle drops near the cloud top are those freshly formed by cloud droplet coalescence and condensational growth. The few but large drizzle drops near the cloud base are a result of drizzle accretion of cloud droplets and drizzle self-collection. To examine the relationship between drizzle and aerosol number concentration, we separate the problem into two steps: first, we explore the dependence of embryonic drizzle drops on CDNC (given that we have shown a strong positive correlation between N_a and CDNC) to see whether the sources of drizzle drops are affected by N_a. Secondly, we explore the dependence of both cloud base drizzle rate and LWP on CDNC (section 4.4) to see whether drizzle depletes in-cloud water in responses to CDNC changes.

[30] Figure 12a displays the observed relationship between drizzle drop number concentration (N_d) and CDNC. The drizzle drop number concentration is averaged over the upper third of the cloud layer to represent precipitation embryos. The data points in Figure 12a can be basically separated into two groups (by two circles): The cleaner cloud group (CDNC ~70–200 cm^{-3} and N_d ~0.2–0.8 cm^{-3}) clearly is characterized by more drizzle drops than the polluted cloud group (CDNC ~220–350 cm^{-3} and N_d < 0.2 cm^{-3}). There is less distinguishable dependence of N_d on CDNC on Figure 12c. This is because the number of embryonic drizzle drops is influenced both by the CDNC and the LWC amounts. Therefore, multiple regression of these three variables in log-log space yields a beter correlation than that in Figure 12c:

$$N_d = 23.8(\mathrm{CDNC})^{-0.53}(\mathrm{cloud\text{–}and\text{–}drizlle\ LWC})^{1.34}, \quad (R^2 = 0.81). \tag{5}$$

This form of relationship is similar to the *Kessler* [1969] type parameterization of the warm rain autoconversion rate,

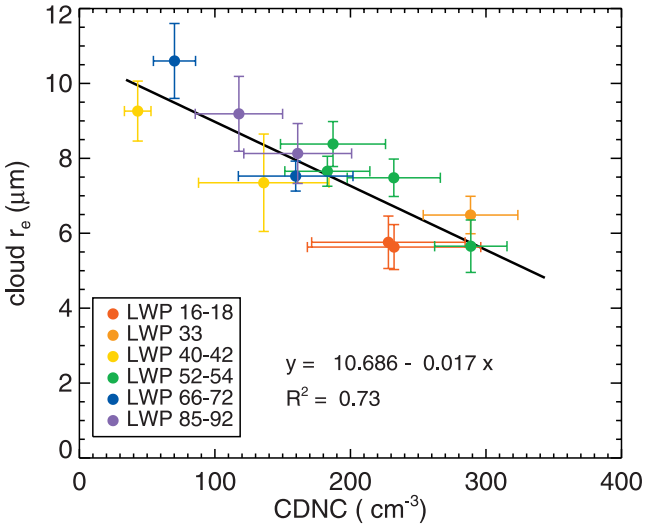

Figure 11. Cloud droplet effective radius versus cloud droplet number concentration. Error bar represents the standard deviation about the mean. Values are from Table 1. Solid line is the linear fit through all clouds. Data are also sorted based on cloud LWP (g m^{-2}) as displayed in the legend.

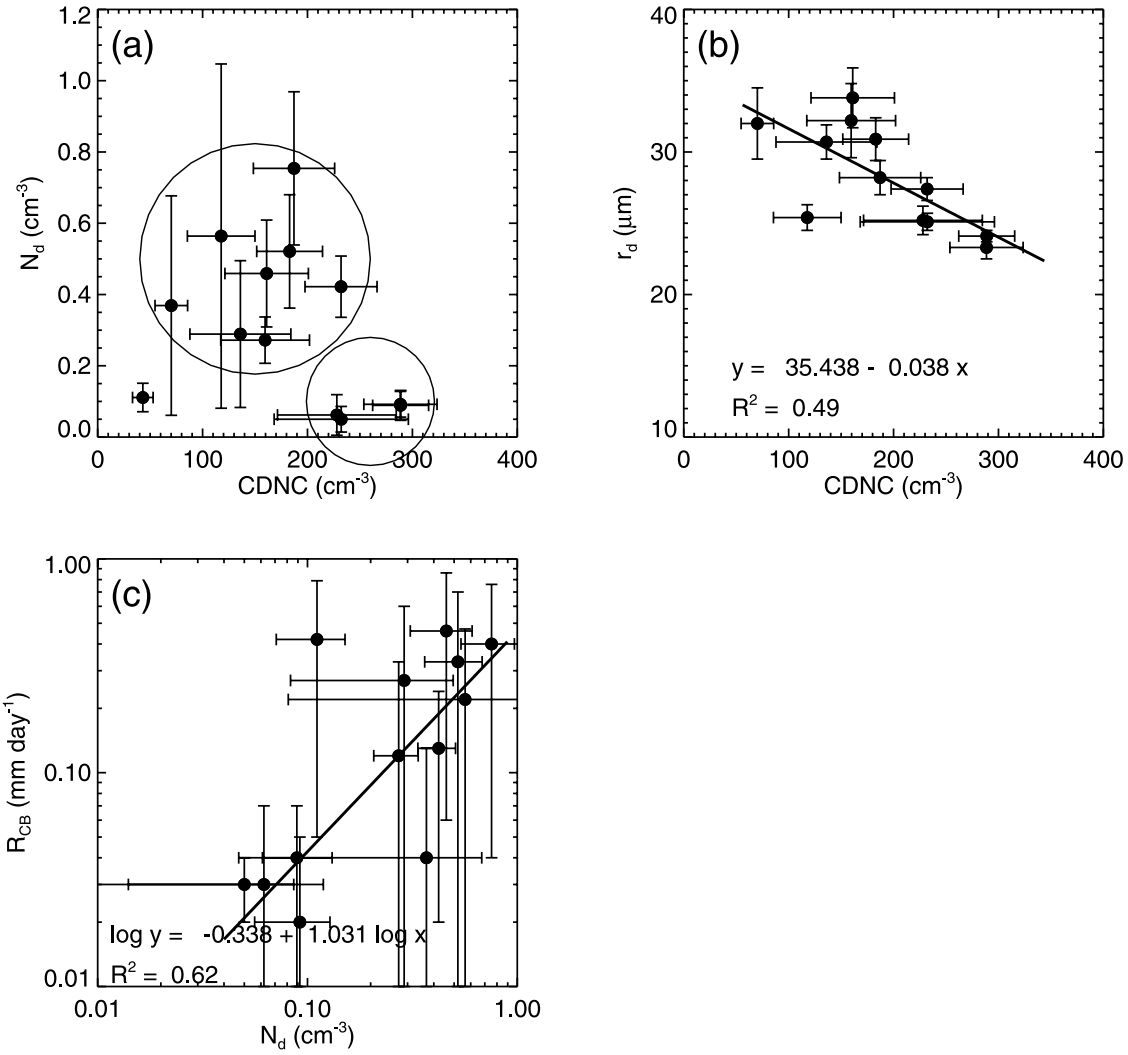

Figure 12. (a) Drizzle drop number concentration (N_d) and (b) drizzle mean radius (r_d) versus cloud droplet number concentration (CDNC). Circles in Figure 12a divide data into two groups. Cloud 10 is excluded from any group. See text for explanation. (c) Relationship of embryonic drizzle drop number concentration and cloud-base drizzle rate. Error bar in each plot is the standard deviation about the mean. Data are from Table 1. The solid lines in Figures 12b and c are regression lines of all clouds except cloud 10. Regression results are also presented.

which is the rate of drizzle drop production employed in numerical models (e.g., *Wood* [2005b]). We note that cloud 10 is not consistent with the other clouds, as it shows particularly low N_d with lowest CDNC. This case also exhibits notably smaller drizzle drops (Figure 12b). It is possible that this case has evident decoupled (discontinuous) features in LWC and CDNC vertical profiles (not shown) and significantly less intensive subcloud turbulence (σ_w in Table 1). Figure 12b shows an anti-correlation between drizzle drop mean radius (r_d) and CDNC with moderate correlation.

[31] As drizzle drops fall below cloud base, cloud LWP is reduced, in the absence of other dynamical changes. The cloud base drizzle rate (R_{CB}) is a proxy for the extent to which drizzle depletes liquid water in cloud. As discussed above, cloud base drizzle drops are formed as a result of collision and coalescence of cloud top embryonic drizzle falling through the cloud layer. Hence R_{CB} shows a strong positive dependence on cloud top N_d (Figure 12c). Together with the correlations for N_d-R_{CB} and CDNC-N_d, it is not surprising that the observational relationship between R_{CB} and CDNC in Figure 13 shows that cleaner clouds have a larger cloud base drizzle rate. In this respect, the current results are consistent with other in situ aircraft data of marine stratocumulus, e.g., the second Dynamics and Chemistry of Marine Stratocumulus (DYCOMS-II) [*van Zanten et al.*, 2005], and the Atlantic Stratocumulus Transition Experiment (ASTEX) first Lagrangian experiment and the U.K. Met Office C-130 aircraft studies [*Wood*, 2005a]. We note that the maximum ensemble-averaged R_{CB} listed in Table 1 is about 0.5 mm day^{-1}, so MASE clouds are classified to exhibit light to moderate drizzle rate based on a 1 mm day^{-1} heavy drizzle threshold [e.g., *Lu and Seinfeld*, 2005 and *van Zanten et al.*, 2005]. Summarizing Figures 12 and 13, the MASE data show that more polluted (thereby higher CDNC) clouds have fewer and

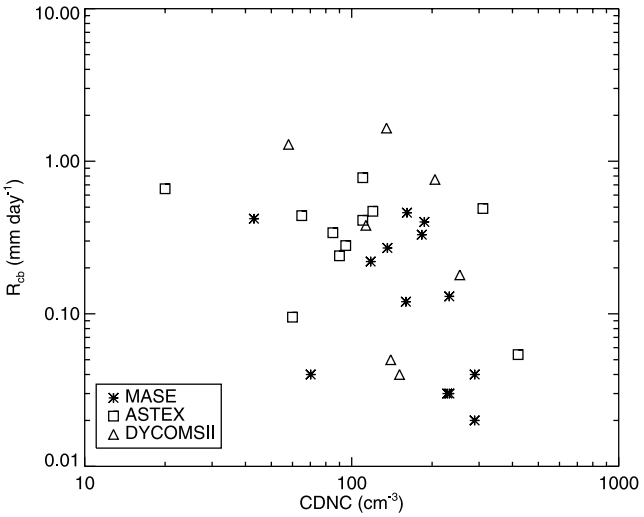

Figure 13. Cloud base drizzle rate (R_{CB}) versus cloud droplet number concentration. DYCOMS II data are from the work of *van Zanten et al.* [2005]. Data labeled ASTEX are from ASTEX and U.K. Met Ofice C-130 [*Wood*, 2005a].

smaller drizzle drops near cloud top and a smaller cloud base drizzle rate than their cleaner counterparts, which exemplifies drizzle suppression by pollution.

4.4. Ensemble-Averaged Liquid Water Path

[32] The ensemble-averaged LWP as a function of subcloud aerosol number concentration is displayed in Figure 14. In this figure, the cloud depth (H)-adjusted mean LWC, the ratio of LWP to H, is used as a surrogate for LWP, so that the dependence of LWP on H is eliminated. The amount of drizzle LWP is significantly less (the difference between the circles and triangles) for the two most polluted clouds.

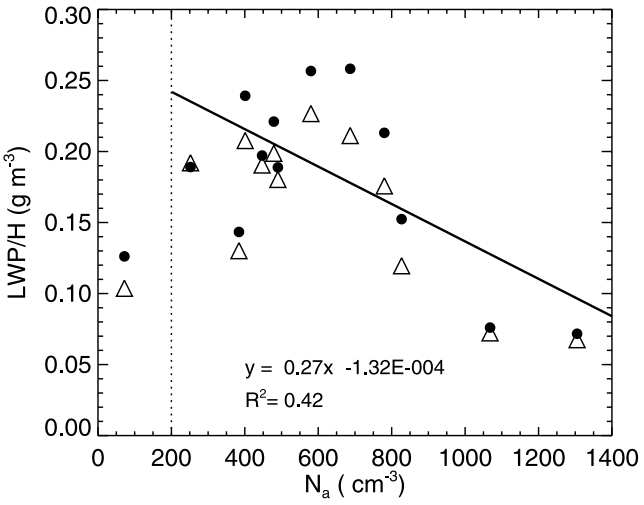

Figure 14. Ratio of liquid water path to cloud depth as a function of subcloud aerosol number concentration. Solid circles represent cloud-and-drizzle LWP, and triangles represent cloud LWP. Values are from Table 1. Solid line is the regression result of the solid circle data excluding those to the left of the dotted line (N_a = 200 cm^{-3}).

The entire data set appears to be separable into two groups (dotted line) at N_a = 200 cm^{-3}. For conditions with N_a > 200 cm^{-3}, there exists a clear negative correlation of either cloud or cloud-and-drizzle LWP with N_a; that is, the more polluted cloud has a smaller cloud LWP. Even though evidence is found for drizzle suppression, the MASE clouds exhibit a weak to moderate drizzle rate so that drizzle does not appear to deplete enough in-cloud LWP to

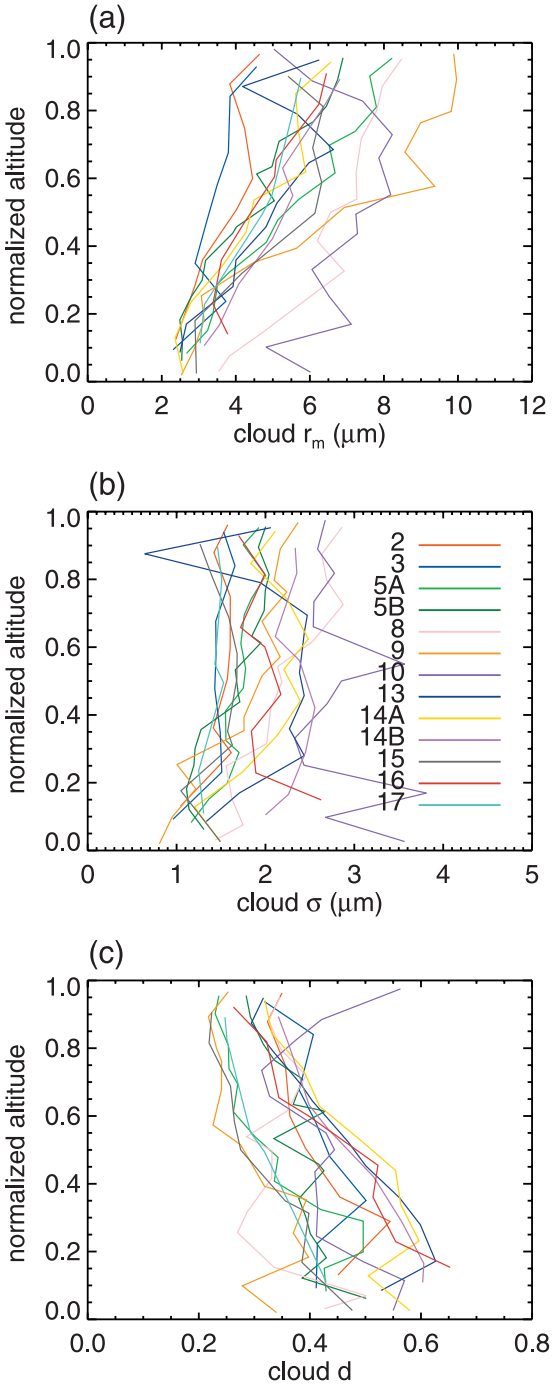

Figure 15. Vertical profiles of (a) cloud droplet mean radius, (b) cloud droplet spectral width, and (c) cloud droplet relative dispersion. The vertical axis is the normalized altitude relative to cloud depth. Data are averaged over the cloudy region.

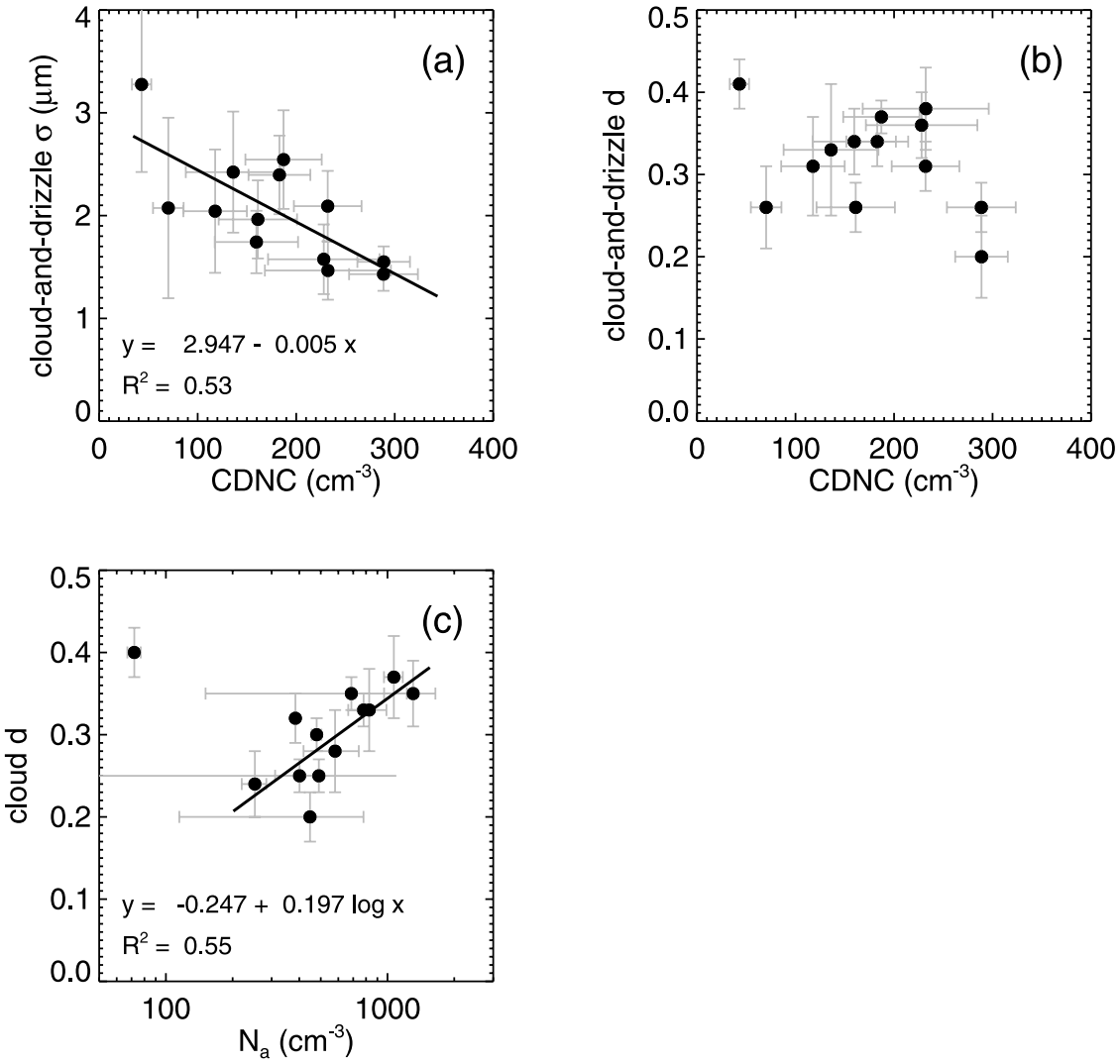

Figure 16. (a) Cloud-and-drizzle drop spectral width and (b) cloud-and-drizzle drop relative dispersion versus cloud droplet number concentration. (c) Cloud drop relative dispersion versus subcloud aerosol number concentration. Solid line in Figure 16a is the regression result of all 13 clouds, while in Figure 16c, cloud 10 is excluded from the regression.

produce a positive LWP-versus-N_a relationship. This indicates that when the cloud base drizzle is weak, drizzle has negligible impact on the MBL moisture budget, which is then more likely determined by the cloud top entrainment drying [*Ackerman et al.*, 2004; *Lu and Seinfeld*, 2005]. There is, however, a hint of a positive LWP-versus-N_a relationship by comparing the LWP of the cleanest cloud (cloud 10, $N_a < 200$ cm^{-3}) with those of $N_a = 200$–850 cm^{-3}. Cloud 10 occurred in a decoupled MBL with relatively weaker subcloud turbulence than other clouds (Table 1). On the basis of only one cloud, one cannot draw an overly general conclusion.

[33] Extracting any simple and direct mechanism of LWP reduction by drizzle is complicated by drizzle intensity, evaporation of drizzle below cloud base, and dynamical adjustment of cloud when drizzling, so the above conclusions should be viewed with caution.

4.5. Ensemble-Averaged Droplet Spectral Dispersion

[34] *Lu and Seinfeld* [2006] carried out LES simulations of marine stratocumulus and investigated the factors that control the cloud droplet spectral relative dispersion in response cloud doplet soctral relative dispersion to increasing aerosol number concentration. They found that cloud spectral relative dispersion decreases with increasing aerosol number concentration particularly at low N_a ($N_a \leq$ 1000 cm^{-3}), in agreement with the observational data derived from the work of *Miles et al.* [2000] of 17 separate studies. They showed that this trend of decreasing d with increasing N_a is a result of more rapid decrease of σ than r_m with N_a. They also found that the coefficient k depends inversely on d. They attributed this result to suppressed drizzle at increased aerosol loading, which results in less collision and coalescence spectral broadening and more spectral narrowing by droplet condensational growth at

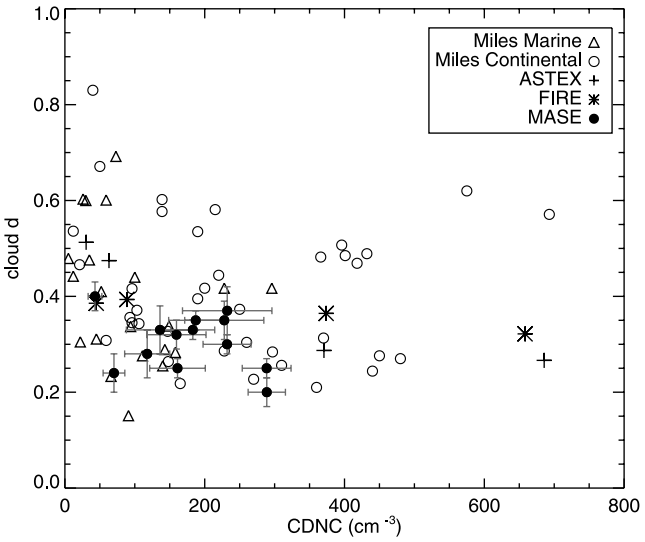

Figure 17. Cloud relative dispersion versus cloud droplet number concentration. MASE data are from Table 1. MASE relative dispersion is averaged over the upper third of the cloud depth. FIRE and ASTEX data are simulation results from *Lu and Seinfeld* [2006], averaged over the cloud depth. Marine and Continental data are observations of stratiform clouds compiled by *Miles et al.* [2000], and those data far from cloud top are removed for consistency.

higher updraft velocities dynamically induced by suppressed drizzle.

[35] Ensemble-averaged vertical profiles of cloud mean radius, cloud spectral width, and relative dispersion are shown in Figure 15 and compared against data from ACE2 [*Pawlowska et al.*, 2006]. Both MASE (Figure 15a) and ACE2 (their Figures 2 and 3) show r_m increases with altitude. Most clouds sampled in MASE start with r_m of 2.5–3.5 μm at cloud base, and grow into a larger range of 4.5–10 μm in response to variations in N_a. Vertical profiles of σ (Figure 15b) are generally nearly constant with height, with some cases showing a slight increasing trend with altitude near cloud top (clouds 5A, 5B, 8, 9, and 14). These features are consistent with the polluted clouds (both adiabatic and nonadiabatic regions) and clean clouds (in the nonadiabatic regions) of ACE2 [*Pawlowska et al.*, 2006]. Unlike the nondrizzling stratocumulus described in *Martin et al.* [1994], in which relative dispersion is constant with height, data from both MASE and ACE2 show vertical variations in d. The MASE vertical profiles of d are similar (Figure 15c, except cloud 10) to that of the ACE2 marine cloud (their Figure 2), in which dispersion decreases with increasing altitude. The large value of d near cloud base is a result of cloud base mixing and updraft velocity variance. We also note that MASE vertical profiles show $d = 0.2–0.6$ for 13 clouds, while the ACE2 marine cloud shows $d = 0.1–0.2$. (The smaller vertical variation in d for ACE2 might be due to the fact that there is only marine cloud considered).

[36] The relative dispersion calculated over the combined cloud and drizzle drop spectra is larger than that calculated over the cloud spectrum only (Table 1), and the difference is roughly proportional to the drizzle drop number concentration.

[37] The ensemble-averaged values of cloud and drizzle combined spectral width (cloud-and-drizzle σ) versus CDNC (Figure 16a) show that cleaner clouds (low CDNC) have broader spectral width. The mean radius (r_m) is similar to r_e that decreases with CDNC or N_a (not shown). However, the relationship between cloud-and-drizzle d with CDNC in Figure 16b is less obvious. We note that the data can be roughly separated into three groups: a particularly high value of d for the cleanest cloud (cloud 10, $d = 0.41$), a relatively small value of d for the two points at CDNC $\approx$ 280 cm^{-3} (cloud 15, $d = 0.20$; cloud 17, $d = 0.26$), and in between, a group of data points with medium value of d. The points in the middle group seem to show a positive correlation between d and CDNC. Although we see less robust patterns in the d-CDNC plot, Figure 17 shows that MASE d values are basically in agreement with observations of several stratiform clouds in the study of *Miles et al.* [2000] and LES simulations of the First International Satellite Cloud Climatology Project Regional Experiment (FIRE) and ASTEX [*Lu and Seinfeld*, 2006]. This figure also shows that d is relatively larger for CDNC <100 cm^{-3} than d for CDNC >100 cm^{-3}. The impact of aerosol number concentration on cloud relative dispersion can be best represented by the plot of d-N_a because N_a is the basic parameter for the level of pollution and CDNC is indirectly determined by N_a and updraft velocity. The d-N_a relation is presented in Figure 16c, which shows a positive correlation between d and N_a. The ensemble-averaged results seem to suggest that more polluted clouds have a larger relative dispersion, in agreement with other flight-averaged data [*Martin et al.*, 1994; *Liu and Daum*, 2002; *Pawlowska et al.*, 2006]. However, it should be pointed out that studies by *Liu and Daum* [2002] and *Pawlowska et al.* [2006] use CDNC instead of N_a as the basis for the dispersion correlation. On the basis of the good relationship of ensemble-averaged results of d-N_a and the previous reasoning, we suggest that d-N_a maybe a better surrogate for the dispersion effect. We also note that the "in-flight" relationship of d-CDNC for MASE and ACE2 [*Pawlowska et al.*, 2006] as analyzed in section 3.4 shows the opposite trend from the "ensemble-averaged" relationship of d-N_a shown here. The LES study of *Lu and Seinfeld* [2006] under the same sounding profile also predicts the in-flight relationship between d and N_a. These results suggest that the ensemble-averaged relationships between d and N_a (or CDNC) are affected not only by N_a but also by dynamical conditions such as cloud base updraft velocity and cloud top mixing, which vary between cloud cases because of different sampling locations (Table 1).

[38] The coefficient k is calculated over the upper third of the cloud depth following the same reasoning as for the effective radius. The flight-averaged cloud (cloud-and-drizzle) k is shown to correlate highly with cloud (cloud-and-drizzle) d (Figure 18a); which suggests that relative dispersion is a suitable proxy for parameterization of k. For this reason, the scatterplot of cloud-and-drizzle k versus CDNC (Figure 18b), is similar to that of d versus CDNC, which shows no simple dependence. It is shown that k is smaller for those cases with CDNC <250 cm^{-3} than k for CDNC >250 cm^{-3}. The k-N_a relationship is

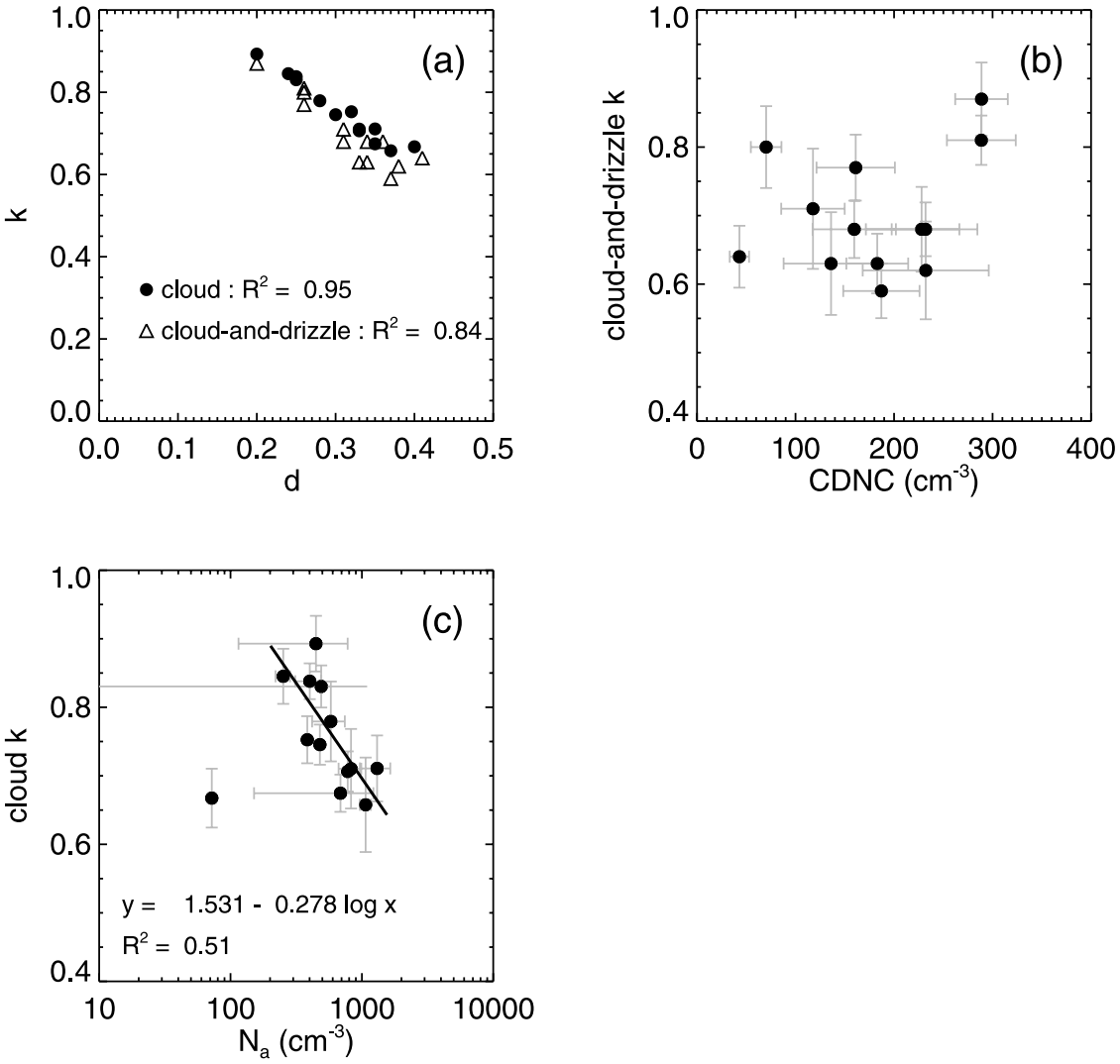

Figure 18. Observed cloud drop dispersion. (a) k versus cloud (cloud-and-drizzle) relative dispersion. Correlation is also presented. (b) Cloud-and-drizzle k versus cloud droplet number concentration. (c) Cloud k versus subcloud aerosol number concentration. Solid line is the regression line through all clouds except cloud 10. Data presented are from Table 1.

shown in Figure 18c; as expected from results of d, k shows a strong inverse dependence with N_a. For cloud with N_a about 1000 cm^{-3}, k is about 0.65–0.7, and for N_a = 300–400 cm^{-3}, k is about 0.8. MASE flight-averaged results are close to the analysis of stratocumulus by *Martin et al.* [1994], who showed cloud k = 0.67 for continental cloud (aerosol number concentration = 375–1500 cm^{-3}) and k = 0.80 for maritime cloud (aerosol number concentration = 36–280 cm^{-3}). However, again, the regression between k and N_a has been performed in an N_a region that is close to Martin's continental cloud conditions.

5. Summary and Conclusion

[39] The MASE field campaign was undertaken in July 2005 to evaluate aerosol-cloud relationships in the climatically important regime of eastern Pacific marine stratocumulus. Thirteen clouds sampled in the region 123.5–121.5°W and 35.75–36.75°N were selected for detailed analysis; subcloud aerosol number concentrations varied from 70 to 1300 cm^{-3}, with some cases exhibiting ship tracks. Among the clouds sampled, that observed on July 5 was clearly impacted by a ship track, as confirmed by in situ aircraft measurements and GOES near-IR satellite imagery. Multiple airborne horizontal traverses (~30 km) through the ship track and unperturbed regions provide insights into variations of cloud properties on a 50-m (~1 Hz) scale both horizontally and vertically. Comparison of ship track and clean regions in the upper portion of the cloud shows that the ship track region exhibited a smaller cloud drop effective radius, reduced drizzle drop number concentration, and larger cloud LWC than the adjacent clean regions. Therefore the data from this cloud provide evidence for the first indirect effect, as well as drizzle suppression by enhanced aerosol number concentration and corresponding larger cloud LWC as a consequence of reduced depletion of cloud water by drizzle. The ship track region also exhibits a smaller cloud drop spectral width and relative dispersion, in

accord with LES predictions of *Lu and Seinfeld* [2006] based on meteorological conditions in the ASTEX and FIRE experiments.

[40] The ensemble average of aerosol and cloud conditions over the 13 cloud regions sampled were also computed. For these, as subcloud aerosol number concentration increases, cloud drop number concentration increases. The magnitudes of aerosol and cloud drop number concentrations and their dependences lie roughly in the range as those reported by *Martin et al.* [1994] for a variety of locations. Averaging over all 13 clouds, as N_a (or CDNC) increases, the cloud drop effective radius decreases, a robust demonstration of the Twomey effect.

[41] Drizzle was prevalent in virtually all the clouds sampled. Drizzle drops were found to be most numerous and smallest near cloud top. The data suggest that more polluted clouds have fewer embryonic drizzle drops near cloud top, resulting in a smaller cloud base drizzle rate. The smaller cloud base drizzle rate, however, does not result in a larger LWP when compared with the clean clouds. It appears that direct conversion of cloud drops to drizzle is insufficient to explain the dependence of LWP on aerosol number concentration; drizzle intensity and the dynamic adjustment of the cloud in response to drizzle in-cloud latent heating, subcloud evaporative cooling, and cloud top entrainment would need to be taken into consideration [*Ackerman et al.*, 2004; *Lu and Seinfeld*, 2005].

[42] Averaged results over all 13 clouds show that more polluted clouds have narrower spectral width. The MASE data exhibit a clear positive correlation between cloud drop spectral dispersion d as a function of N_a.

[43] In general, on the ensemble cloud scale, increases in aerosol number concentration result in cloud LWP decreases and dispersion broadening acting together to diminish the Twomey effect; while on the scale of a single ship track-perturbed cloud, cloud LWP enhancement and dispersion narrowing act to increase the overall aerosol indirect effects. The contrast is due to the fact that, at the ensemble scale, clouds are influenced by different meteorological conditions that result in different cloud top entrainment, cloud base updraft variance, drizzle intensity, and surface evaporation; at the scale of a single cloud, the ship track and clean regions are embedded in the similar sounding profile, and the aerosol-induced changes are compared irrespective of the variations in LWP and dispersion due to ambient conditions.

Appendix A: Data Analysis

[44] The instrumentation payload on the Twin Otter aircraft is listed in Table 2. The nominal airspeed of the Twin Otter is 50 m s^{-1}. Figure 1 shows the flight path on 5 July 2005; this flight path was typical of those in the experiment. Below- and above-cloud aerosols were measured, both size and composition. Cloud droplet size distributions were measured by the forward scattering spectrometer probe (FSSP), and cloud droplets are defined as those having radius greater than 1.56 μm and smaller than drizzle drops. Drizzle drop size distribution was measured by the cloud-imaging probe (CIP), and drizzle drops are typically defined as those having radius greater than 20 μm. Cloud base and top are determined using the FSSP threshold of >5 cm^{-3}, LWC >0.001 g cm^{-3}, and RH must be greater than 100%. The aerosol number concentration, N_a, was obtained by the CPC. Wind velocities were measured by the five-hole turbulence probe on the nose of the aircraft, C-MIGITS or TANS-Vector inertial navigation systems, and C-MIGITS or Nova Tel GPS following *Lenschow* [1986]. A Gaussian filter was applied to the vertical wind velocity data to remove any long-period (scale greater than 2.5 km) drift possibly associated with unmeasured changes in the aircraft state. The standard deviation of cloud base updraft velocity (σ_w) is calculated by the standard deviation of vertical velocity >0 along the flight leg near cloud base.

[45] For the ensemble-averaged cloud properties presented in section 4, we first calculate the mean value of cloud properties (e.g., CDNC, ...etc.) in each altitude section of 30 m, and then perform the vertical average. Cloud droplet number concentrations are averaged over the cloud depth. Liquid water path is calculated by vertically integrating the averaged liquid water content in each altitude bin of 30 m. Drizzle drop number concentration, cloud LWC effective radius, relative dispersion, and k coefficient are averaged over the upper third of cloud depth. Drizzle rate is averaged over the lower third of cloud depth.

[46] **Acknowledgments.** This work was supported by the Office of Naval Research (N-00014-04-1-0018) and National Science Foundation grant ATM-0340832. PILS data were provided by Armin Sorooshian. We appreciate valuable comments from Patrick Chuang and Robert Wood.

References

Ackerman, A. S., O. B. Toon, D. E. Stevens, and J. A. Coakley (2003), Enhancement of cloud cover and suppression of nocturnal drizzle in stratocumulus polluted by haze, *Geophys. Res. Lett.*, *30*(7), 1381, doi:10.1029/2002GL016634.

Ackerman, A. S., M. P. Kirkpatrick, D. E. Stevens, and O. B. Toon (2004), The impact of humidity above stratiform clouds on indirect aerosol climate forcing, *Nature*, *432*, 1014–1017.

Albrecht, B. A. (1989), Aerosols, cloud microphysics, and fractional cloudiness, *Science*, *245*, 1227–1230.

Brenguier, J. L., H. Pawlowska, L. Schuller, R. Preusker, J. Fischer, and Y. Fouquart (2000), Radiative properties of boundary layer clouds: Droplet effective radius versus number concentration, *J. Atmos. Sci.*, *57*, 803–821.

Breon, F. M., D. Tanre, and S. Generoso (2002), Aerosol effect on cloud droplet size monitored from satellite, *Science*, *295*, 834–838.

Bretherton, C. S., T. Uttal, C. W. Fairall, S. E. Yuter, R. A. Weller, D. Baumgardner, K. Comstock, R. Wood, and G. B. Raga (2004), The EPIC 2001 stratocumulus study, *Bull. Am. Meteorol. Soc.*, *85*, 967–977.

Coakley, J. A., R. L. Bernstein, and P. A. Durkee (1987), Effect of ship-stack effluents on cloud reflectivity, *Science*, *237*, 1020–1022.

Durkee, P. A., R. E. Chartier, A. Brown, E. J. Trehubenko, S. D. Rogerson, C. Skupniewicz, K. E. Nielsen, S. Platnick, and M. D. King (2000a), Composite ship track characteristics, *J. Atmos. Sci.*, *57*, 2542–2553.

Durkee, P. A., K. J. Noone, and R. T. Bluth (2000b), The Monterey Area Ship Track experiment, *J. Atmos. Sci.*, *57*, 2523–2541.

Durkee, P. A., et al. (2000c), The impact of ship-produced aerosols on the microstructure and albedo of warm marine stratocumulus clouds: A test of MAST hypotheses 1i and 1ii, *J. Atmos. Sci.*, *57*, 2554–2569.

Feingold, G., B. Stevens, W. R. Cotton, and R. L. Walko (1994), An explicit cloud microphysics/LES model designed to simulate the Twomey effect, *Atmos. Res.*, *33*, 207–233.

Feingold, G., R. Boers, B. Stevens, and W. R. Cotton (1997), A modeling study of the effect of drizzle on cloud optical depth and susceptibility, *J. Geophys. Res.*, *102*, 13,527–13,534.

Feingold, G., W. L. Eberhard, D. E. Veron, and M. Previdi (2003), First measurements of the Twomey indirect effect using ground-based remote sensors, *Geophys. Res.*, 30.

Feingold, G., R. Furrer, P. Pilewskie, L. A. Remer, Q. L. Min, and H. Jonsson (2006), Aerosol indirect effect studies at Southern Great Plains during the May 2003 Intensive Operations Period, *J. Geophys. Res.*, *111*, D05S14, doi:10.1029/2004JD005648.

Ferek, R. J., D. A. Hegg, and P. V. Hobbs (1998), Measurements of ship-induced tracks in clouds off the Washington coast, *J. Geophys. Res.*, *103*, (D18), 23,199–23,206.

Ferek, R. J., et al. (2000), Drizzle suppression in ship tracks, *J. Atmos. Sci.*, *57*, 2707–2728.

Han, Q. Y., W. B. Rossow, J. Chou, and R. M. Welch (1998), Global survey of the relationships of cloud albedo and liquid water path with droplet size using ISCCP, *J. Clim.*, *11*, 1516–1528.

Han, Q. Y., W. B. Rossow, J. Zeng, and R. Welch (2002), Three different behaviors of liquid water path of water clouds in aerosol-cloud interactions, *J. Atmos. Sci.*, *59*, 726–735.

Hudson, J. G., and S. S. Yum (1997), Droplet spectral broadening in marine stratus, *J. Atmos. Sci.*, *54*, 2642–2654.

Jiang, H. L., G. Feingold, W. R. Cotton, and P. G. Duynkerke (2001), Large-eddy simulations of entrainment of cloud condensation nuclei into the Arctic boundary layer: May 18, 1998, FIRE/SHEBA case study, *J. Geophys. Res.*, *106*, 15,113–15,122.

Jiang, H. L., G. Feingold, and W. R. Cotton (2002), Simulations of aerosol-cloud-dynamical feedbacks resulting from entrainment of aerosol into the marine boundary layer during the Atlantic Stratocumulus Transition Experiment, *J. Geophys. Res.*, *107*(D24), 4813, doi:10.1029/2001JD001502.

Kaufman, Y. J., and T. Nakajima (1993), Effect of Amazon smoke on cloud microphysics and albedo—Analysis from satellite imagery, *J. Appl. Meteorol.*, *32*, 729–744.

Kaufman, Y. J., I. Koren, L. A. Remer, D. Rosenfeld, and Y. Rudich (2005), The effect of smoke, dust, and pollution aerosol on shallow cloud development over the Atlantic Ocean, *Proc. Natl. Acad. Sci. USA*, *102*, 11,207–11,212.

Kessler, E. (1969), On the distribution and continuity of water substance in the atmospheric circulations, *Meteorol. Monogr.*, *32*, 84.

Kim, B. G., S. E. Schwartz, M. A. Miller, and Q. L. Min (2003), Effective radius of cloud droplets by ground-based remote sensing: Relationship to aerosol, *J. Geophys. Res.*, *108*(D23), 4740, doi:10.1029/2003JD003721.

Kogan, Z. N., Y. L. Kogan, and D. K. Lilly (1996), Evaluation of sulfate aerosols indirect effect in marine stratocumulus clouds using observation-derived cloud climatology, *Geophys. Res. Lett.*, *23*, 1937–1940.

Kogan, Z. N., Y. L. Kogan, and D. K. Lilly (1997), Cloud factor and seasonality of the indirect effect of anthropogenic sulfate aerosols, *J. Geophys. Res.*, *102*, 25,927–25,939.

Lenschow, D. H. (1986), *Probing the Atmospheric Boundary Layer*, American Meteorological Society, Boston.

Liu, Y. G., and P. H. Daum (2002), Anthropogenic aerosols: Indirect warming effect from dispersion forcing, *Nature*, *419*, 580–581.

Lohmann, U., and J. Feichter (2005), Global indirect aerosol effects: A review, *Atmos. Chem. Phys.*, *5*, 715–737.

Lu, M.-L., and J. H. Seinfeld (2005), Study of the aerosol indirect effect by large-eddy simulation of marine stratocumulus, *J. Atmos. Sci.*, *62*, 3909–3932.

Lu, M.-L., and J. H. Seinfeld (2006), Effect of aerosol number concentration on cloud droplet dispersion: A large-eddy simulation study and implications for aerosol indirect forcing, *J. Geophys. Res.*, *111*, D02207, doi:10.1029/2005JD006419.

Martin, G. M., D. W. Johnson, and A. Spice (1994), The measurement and parameterization of effective radius of droplets in warm stratocumulus clouds, *J. Atmos. Sci.*, *51*, 1823–1842.

Miles, N. L., J. Verlinde, and E. E. Clothiaux (2000), Cloud droplet size distributions in low-level stratiform clouds, *J. Atmos. Sci.*, *57*, 295–311.

Nakajima, T., A. Higurashi, K. Kawamoto, and J. E. Penner (2001), A possible correlation between satellite-derived cloud and aerosol microphysical parameters, *Geophys. Res. Lett.*, *28*, 1171–1174.

Paluch, I. R., and D. H. Lenschow (1991), Stratiform cloud formation in the marine boundary-layer, *J. Atmos. Sci.*, *48*, 2141–2158.

Pawlowska, H., W. W. Grabowski, and J.-L. Brenguier (2006), Observations of the width of cloud droplet spectra in stratocumulus, *Geophys. Res. Lett.*, *33*, L19810, doi:10.1029/2006GL026841.

Peng, Y. R., and U. Lohmann (2003), Sensitivity study of the spectral dispersion of the cloud droplet size distribution on the indirect aerosol effect, *Geophys. Res. Lett.*, *30*(10), 1507, doi:10.1029/2003GL017192.

Pincus, R., and M. B. Baker (1994), Effect of precipitation on the albedo susceptibility of clouds in the marine boundary-layer, *Nature*, *372*, 250–252.

Rosenfeld, D. (1999), TRMM observed first direct evidence of smoke from forest fires inhibiting rainfall, *Geophys. Res. Lett.*, *26*, 3105–3108.

Rosenfeld, D. (2000), Suppression of rain and snow by urban and industrial air pollution, *Science*, *287*, 1793–1796.

Rosenfeld, D., Y. J. Kaufman, and I. Koren (2006), Switching cloud cover and dynamical regimes from open to closed Benard cells in response to the suppression of precipitation by aerosols, *Atmos. Chem. Phys.*, *6*, 2503–2511.

Schreier, M., A. A. Kokhanovsky, V. Eyring, L. Bugliaro, H. Mannstein, B. Mayer, H. Bovensmann, and J. P. Burrows (2006), Impact of ship emissions on the microphysical, optical and radiative properties of marine stratus: A case study, *Atmos. Chem. Phys.*, *6*, 4925–4942.

Schwartz, S. E., and C. M. Benkovitz (2002), Influence of anthropogenic aerosol on cloud optical depth and albedo shown by satellite measurements and chemical transport modeling, *Proc. Natl. Acad. Sci. USA*, *99*, 1784–1789.

Slingo, A., and H. M. Schrecker (1982), On the shortwave radiative properties of stratiform water clouds, *Q. J. R. Meteorol. Soc.*, *108*, 407–426.

Stevens, B., W. R. Cotton, G. Feingold, and C. H. Moeng (1998), Large-eddy simulations of strongly precipitating, shallow, stratocumulus-topped boundary layers, *J. Atmos. Sci.*, *55*, 3616–3638.

Taylor, J. P., M. D. Glew, J. A. Coakley, W. R. Tahnk, S. Platnick, P. V. Hobbs, and R. J. Ferek (2000), Effects of aerosols on the radiative properties of clouds, *J. Atmos. Sci.*, *57*, 2656–2670.

Twomey, S. (1977), Influence of pollution on shortwave albedo of clouds, *J. Atmos. Sci.*, *34*, 1149–1152.

van Zanten, M. C., B. Stevens, G. Vali, and D. H. Lenschow (2005), Observations of drizzle in nocturnal marine stratocumulus, *J. Atmos. Sci.*, *62*, 88–106.

Warner, J. (1968), A reduction in rainfall associated with smoke from sugarcane fires—An inadvertent weather modification?, *J. Appl. Meteorol.*, *7*, 247–251.

Warner, J., and S. Twomey (1967), Production of cloud nuclei by cane fires and effect on cloud droplet concentration, *J. Atmos. Sci.*, *24*, 704–706.

Wood, R. (2005a), Drizzle in stratiform boundary layer clouds. Part 1: Vertical and horizontal structure, *J. Atmos. Sci.*, *62*, 3011–3033.

Wood, R. (2005b), Drizzle in stratiform boundary layer clouds. Part II: Microphysical aspects, *J. Atmos. Sci.*, *62*, 3034–3050.

W. C. Conant, Department of Atmospheric Sciences, University of Arizona, Tucson, AZ, USA.

R. C. Flagan and J. H. Seinfeld, Departments of Chemical Engineering and Environmental Science and Engineering, California Institute of Technology, Pasadena, 1200 East California Blvd., Mail Code 210-41, Pasadena, CA 91125, USA. (seinfeld@caltech.edu)

H. H. Jonsson, Naval Postgraduate School, Monterey, CA, USA.

M.-L. Lu, Department of Environmental Science and Engineering, California Institute of Technology, Pasadena, CA, USA.

V. Varutbangkul, Department of Chemical Engineering, California Institute of Technology, Pasadena, CA, USA.